Chapter 9

Hydrocarbon Gases from Giant Piston Cores in the Northern Gulf of Mexico: Results from the IMAGES VIII/ PAGE 127 cruise of the RV Marion Dufresne, July 2002

Thomas D. Lorenson[1], Jennifer A. Dougherty[1], and James G. Flocks[2]

Hydrocarbon gases from giant piston cores in the northern Gulf of Mexico: Results from the IMAGES VIII/PAGE 127 cruise of the RV Marion Dufresne*, July 2002; chapter 9* in *Winters, W.J., Lorenson, T.D., and Paull, C.K., eds., 2007, Initial report of the IMAGES VIII/PAGE 127 gas hydrate and paleoclimate cruise on the RV* Marion Dufresne *in the Gulf of Mexico, 2–18 July 2002: U.S. Geological Survey Open-File Report 2004–1358.*

Abstract

Hydrocarbon gases and carbon dioxide (CO_2) extracted from sediment cores from the northern Gulf of Mexico in four distinct regions were studied to constrain the possible occurrence and source of gas that may form gas hydrate. Three sample types were analyzed: gas from dissociated gas hydrate, dissolved gas in sediment, and free gas evolved from sediment collected from gas voids in the core liner.

Gas hydrate was recovered in four cores from previously known venting sites about 3 to 9 meters below the sea floor but was not found in adjacent basins. Gas hydrate samples were preserved for analysis from only one core—MD02-2569 in the thalweg of Mississippi Canyon within lease area MC802. The quality of the gas hydrate recovered was poor because the time for core recovery and sampling approached 2 hours. Methane, ranging from 95.0 to 99.5 percent, is the principal gas in the gas hydrate with concentrations of CO_2 ranging from 0.16 to 4.0 percent. Higher molecular weight hydrocarbon gases—ethane, propane, and isobutane—are found in concentrations exceeding 1,000 parts per million, suggesting that both structure I and structure II gas hydrate are present.

Sediment collected near the summit of a 1- to 1.5-kilometer-diameter sea-floor mound on Kane Spur within lease area MC853 (34 kilometers east of MC802) contained visible oil and hydrocarbon gases of thermogenic origin. Sediment from MC802 contained some proportion of hydrocarbon gases of likely thermogenic origin but at much lower concentrations than at MC853. Free gas from sediment at MC853 also was composed of mainly thermogenic hydrocarbons. Sediment gases from other areas (Tunica Mound, Bush Hill, and areas in and flanking Mississippi Canyon) were composed mainly of microbial methane with traces of thermogenic hydrocarbons.

Introduction

The northern Gulf of Mexico hosts numerous sea-floor (<7-meter (m) subbottom) occurrences of gas hydrate. The sea floor is dominated by salt-tectonic basin structures, high sedimentation rates (about 40 centimeters per thousand years (cm/k.y.)), and complex late Neogene stratigraphy with common sea-floor failures. Natural oil and gas seeps are abundant, usually associated with fault conduits that often are capped by gas hydrate when the seeps are within the hydrate stability zone. While gas hydrate is relatively common at the sea floor, the lack of bottom simulating reflections (BSR) on seismic records suggests that gas hydrate at depth is largely absent. Thus, it is unknown if there are significant gas hydrate accumulations in reservoir sediments away from faults. To address this question, a cruise was conducted with the International Marine Past Global Changes Study (IMAGES) and Paleoceanography of the Atlantic and Geochemistry (PAGE) programs aboard the research vessel (RV) *Marion Dufresne* in July 2002 (Lorenson and others, 2002).

Eighteen giant piston cores up to 38 m long and four giant box cores up to 9 m long were recovered along seismic-reflection transects in widely different geologic environments

[1]U.S. Geological Survey, 345 Middlefield Road, MS-999, Menlo Park, CA 94025 USA (tlorenson@usgs.gov).

[2]U.S. Geological Survey, 600 4th Street S., St. Petersburg, FL 33701 USA.

in water depths ranging from 600 to 1,300 m (table 1). The transects were designed to extend from known sea-floor gas hydrate occurrences across the adjacent basin to background sediments away from any gas-venting sites.

The type of dissolved and free hydrocarbon gas in marine sediments that is trapped in gas hydrate determines the hydrate structure and, hence, the pressure and temperature conditions under which it is stable. To this end, we measured the hydrocarbon gas content of sediments and used the data as proxies for methane and other hydrocarbon gas source discrimination, the general gas contents of the sediment, and the likely type of gas hydrate that may have dissociated during the core recovery process.

Table 1. Locations of cores measured for gas composition.

[G, gravity core; GHF, gravity heat-flow core; C2, box core]

Core ID	Latitude	Longitude	Area name
MD02-2535	27.61983	92.24100	Tunica Mound
MD02-2537	27.61600	92.24867	Tunica Mound
MD02-2538GHF	27.61667	92.24717	Tunica Mound
MD02-2539	27.63967	92.19217	Tunica Mound
MD02-2541	27.63250	92.21233	Tunica Mound
MD02-2542GHF	27.63217	92.21200	Tunica Mound
MD02-2543G	27.61233	92.25550	Tunica Mound
MD02-2545G	27.61400	92.25167	Tunica Mound
MD02-2546	27.61567	92.24700	Tunica Mound
MD02-2548	27.63750	92.19950	Tunica Mound
MD02-2553C2	27.18350	91.41667	Pigmy Basin
MD02-2554	27.78333	91.49900	Bush Hill Basin
MD02-2555	27.78317	91.48917	Bush Hill Basin
MD02-2556	27.78300	91.47750	Bush Hill Basin
MD02-2559	28.22250	89.08817	Kane Spur
MD02-2560	28.24333	89.15500	Kane Spur
MD02-2561	28.20517	89.02017	Kane Spur
MD02-2562	28.07983	89.14017	Kane Spur
MD02-2563	28.12333	89.13633	Kane Spur
MD02-2565	28.12350	89.13950	Kane Spur
MD02-2566	28.11917	89.10317	Kane Spur
MD02-2567	28.10017	89.01983	Kane Spur
MD02-2569	28.15217	89.47967	West Mississippi
MD02-2570	29.57100	89.68983	West Mississippi
MD02-2572GHF	28.07100	89.68967	West Mississippi
MD02-2573GHF	28.15200	89.47983	West Mississippi

Methods

Field Sampling

A variety of gas sample types were collected for this study: (1) cored sediment, (2) free gas, and (3) gas produced by controlled dissociation of gas hydrate samples.

Sediment samples destined for gas analysis were prepared using a procedure modified from Kvenvolden and Redden (1980). Cored sediment in a 5-centimeter (cm) interval was cut out, extruded from the core liner, sealed in a 500-milliliter (mL) metal can equipped with a septum, and weighed. The sample can was filled with water to the rim, and 100 mL of water was removed. After 2 to 3 grams of sodium chloride salt was added as a bacterial growth inhibitor, the can was sealed, frozen in the upside-down position, and shipped to the U.S. Geological Survey (USGS) laboratory in Menlo Park, California, for hydrocarbon gas analyses.

In the shore-based laboratory, the frozen samples were thawed in cans until they reached a temperature of about 20 degrees Celsius (°C). They were then placed into a high-speed shaker for 5 minutes. The partitioned hydrocarbon headspace gases were analyzed using a gas chromatograph. Other gas subsamples were withdrawn from the can by using a syringe and were injected into a pre-evacuated 30-mL serum vial for subsequent carbon isotopic analyses.

Free Gas

Free-gas samples were taken when visible signs of sediment extrusion were noticed during routine drilling of gas-venting holes in the core liner. In such instances, “mud-worms” commonly were seen extruding from the holes. Gas was sampled by inserting a valve-tipped plastic syringe into the hole and allowing the gas to expand into the syringe. The gas in the syringe was injected into an evacuated 30-mL serum vial for transport to the laboratory and then analyzed by direct injection onto a gas chromatograph as described below.

Gas Hydrate Analyses

The system for measuring the gas and water content of dissociating gas hydrate consisted of a sample holder, a gauge block, a pressure gauge, and a manifold. The manifold had an interchangeable gas-sampling port with septum or a quick-connection to vacuum, a steel cylinder for collection of gas, and a pressure gauge. The device was first used on Deep Sea Drilling Program Leg 76, and a more complete description of the device can be found in Kvenvolden and others (1984). For each experiment, gas hydrate that was temporarily stored in liquid nitrogen was placed on aluminum foil and broken into smaller sizes. Pieces with minimal sediment were placed into the sample device previously cooled by liquid nitrogen. The system was sealed and the lower portion of the device was placed into a water bath. As the gas hydrate dissociated, pressure inside the device increased, then stabilized. After about

10 minutes of stable pressure, the pressure and the temperature of the water bath were recorded. A valve was opened on the manifold, which allowed the dissociated gas to expand into the sample manifold and the pre-evacuated cylinder. Gas was sampled from the manifold and analyzed by gas chromatography. After gas sampling, the residual water and any sediment were weighed and their respective volumes calculated and subtracted from the volume of the reaction chamber. Gas volumes were calculated according to the ideal gas law at standard temperature and pressure (STP). Residual water was decanted after centrifugation, then sealed, and refrigerated pending chlorinity measurements and isotopic analyses of the water.

Hydrocarbon Gas Composition Determination

A Shimadzu GC-14A gas chromatograph equipped with a Chemipack C-18, 1.8-m x 3.2-millimeter (mm) 80/100 mesh stainless steel column was used to measure C_1-C_8 hydrocarbon gases. The GC-14A is configured with a 1-mL, valve-actuated, sample loop for injection, and a flame ionization detector (FID) for gas detection. Samples were introduced by syringe at atmospheric pressure, and a minimum of 10 mL of gas was used to flush the injection loop. Run conditions were 35 °C for 1.5 minutes increasing at 20 degrees per minute to a constant 150 °C. Helium was used as the carrier gas at a constant mass flow rate of 3 kilograms per square centimeter (kg/cm^2). FID temperature was held at 150 °C.

Results are reported relative to the volume of cuttings or weight of core material from which the gases were extracted, that is, microliters of gas per liter of wet sediment (microliter per liter (µL/L). Gas concentration data are reported for a series of hydrocarbons given in order of elution (table 2, p. 28): methane (C_1), ethane (C_2), propane (C_3), isobutane (iC_4), normal butane (nC_4), neopentane (neoC_5), isopentane (iC_5), normal pentane (nC_5), 2,2 dimethylbutane (2,2MC_4), 2methylpentane (2MC_5), 3methylpentane (3MC_5), normal hexane (nC_6), normal heptane (nC_7), and methylcyclohexane (McC_6). Approximate detection limits for all hydrocarbon compounds are 0.05 parts per million (ppm) by volume corresponding to about 0.02 µL/L.

CO_2 Determination

Carbon dioxide (CO_2) concentrations were determined in the laboratory with a Hewlett-Packard P-200 micro-gas chromatograph equipped with an 8-m-long by 0.32-mm-diameter PoraPlot U column. Run conditions were isothermal at 60 °C with a run time of 2 minutes. Helium carrier gas column head pressure was maintained at 1.25 bar. Compounds were detected with a micro-machined thermal conductivity detector. The approximate detection limit for CO_2 is about 0.5 µL/L. Concentrations of primary gases (nitrogen, oxygen, and argon) were not determined because the samples were exposed to air during recovery and packaging.

Hydrocarbon Gas Isotopic Composition Determination

Stable carbon isotope ratio determinations of C_1, C_2, C_3, iC_4, nC_4, nC_5, and CO_2 were made on a Continuous Flow-Isotope Ratio Mass Spectrometer (Finnigan MAT 252 GC-CF-IRMS) at the School of Earth and Ocean Sciences (SEOS), University of Victoria, Canada.

Samples were introduced by syringe into a Stanford Research Instruments gas chromatograph (GC) by way of a gas sample valve (loop volumes: 10, 100, or 200 µL). Analytes were separated at 40 °C on a 30-m GS-Q column (0.32 mm ID (inner diameter)) with a carrier gas flow of 1.8 milliliter per minute (mL/min) ultra-high purity helium. After gas partitioning on the GC, the gas passed through a CuO/Pt microcombustion oven at 850 °C. This oven quantitatively converts the hydrocarbon gases to carbon dioxide and water. The combusted sample products were then passed through a Nafion™ tube to remove water from the combustion and any that may have been in the carrier gas. The purified CO_2/He pulse was scaled by an open-split interface and then transferred into the GC-C-IRMS. Isotope ratios are referenced to the conventional PeeDee Belemnite (PDB) standard through a known CO_2 isotope standard that is added at the open split to the sample runs several times during the analysis.

For stable carbon isotope ratio measurements on the sample CO_2, the gas was partitioned on the GC as discussed above. The microcombustion oven was bypassed for the CO_2 measurements, but the gas stream was dried, split, and measured by CF-IRMS in a manner similar to the light hydrocarbons.

Regional Descriptions

Sediment cores from the northern Gulf of Mexico in four distinct regions (fig. 1) were analyzed in this study: Tunica Mound, Pigmy Basin, Bush Hill, and the Mississippi Canyon area (Kane Spur and West Mississippi Canyon). Table 1 lists core locations that were analyzed for sediment gas concentration.

Tunica Mound

Garden Banks and Green Canyon are known for locally high sedimentation rates from 7 to 11 meters per thousand years (m/k.y.) for the upper sedimentary section, extensive late Neogene salt deformation, and slope failures with mass-wasting along over-steepened parts of the continental slope (Rowan and Weimer, 1998). Sediment ages in the upper 600–700 meters below sea floor (mbsf) likely are no older than 0.5 million years (m.y.) in the study area (Berryhill and others, 1987; Weimer and others, 1998). This region includes the Tunica Mound and Bush Hill coring sites.

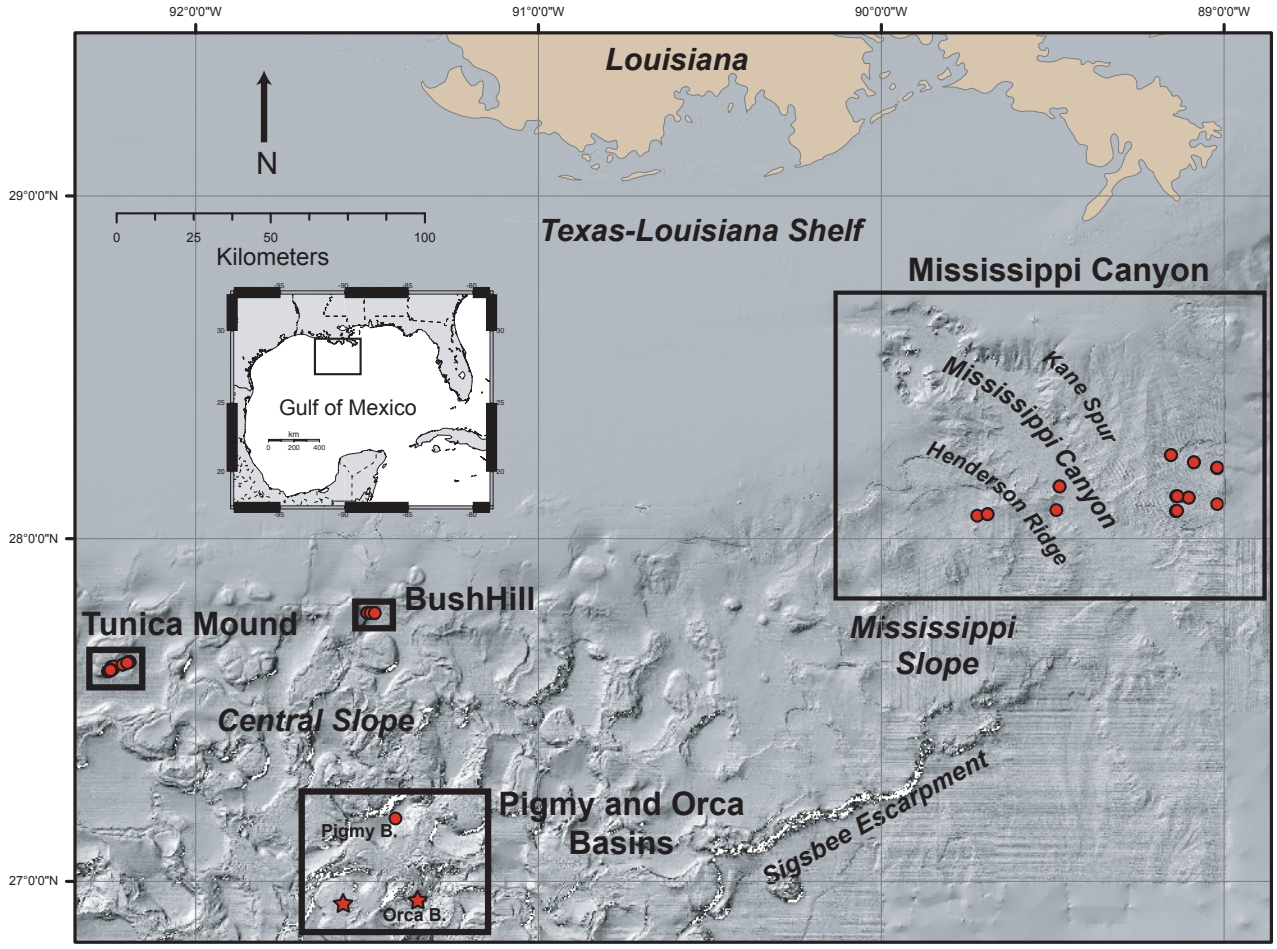

Figure 1. Index map of locations in this report.

The upper sedimentary section of the continental slope, including Tunica Mound, is characterized by layered and chaotic units that are faulted near basin edges and by slope failures on basin flanks. Deformation is greater near salt structures and on over-steepened slopes.

Downslope, well-layered sediments within 300 m of the sea floor have many vertical acoustic "chimney" features, likely small faults, and are bounded by chaotic units directly below and above. The underlying chaotic unit has high reflectivity zones (HRZs) that are dispersed within chaotic stratal units and similar to those in other slope basins at about the same depth (Cooper and Hart, 2003). These gas chimney features extend up from this chaotic unit to the overlying disrupted unit, which has low seismic amplitudes and evidence of faulting and sliding.

Nine gravity and piston cores were taken along a transect along the southern flank of Tunica Mound verging toward but not entering the basin to the east (fig. 2). Tunica Mound is about 14 square kilometers (km^2) in area with a fault running through the southwest to northeast corners. The northwest side of the mound is uplifted in contrast to the southeast corner. The coring transect is about 7 kilometers (km) long at a subparallel angle to the fault in the southeast quadrant. Water depths along the transect range from 580 to 620 m. All sites on the transect remain within the confines of the dome; however, the site to the northeast enters the basin between Tunica Mound and Caddo Mound located to the east of Tunica Mound. Most of the gravity cores were taken on or near a subsidiary mound with seismic features indicative of active fluid flow, including authigenic carbonate, sea-floor relief, and gas. Piston cores were taken away from the submound.

Pigmy and Orca Basins

Cores in Pigmy and Orca Basins were obtained to conduct paleoceanographic research (fig. 3). The basins presumably have similar depositional histories; however, Orca Basin has been covered by a seawater brine for some time causing an anoxic environment and preservation of organic matter. In contrast, Pigmy Basin has been subject to oxic conditions. One sample was analyzed from Pigmy Basin and none from Orca Basin.

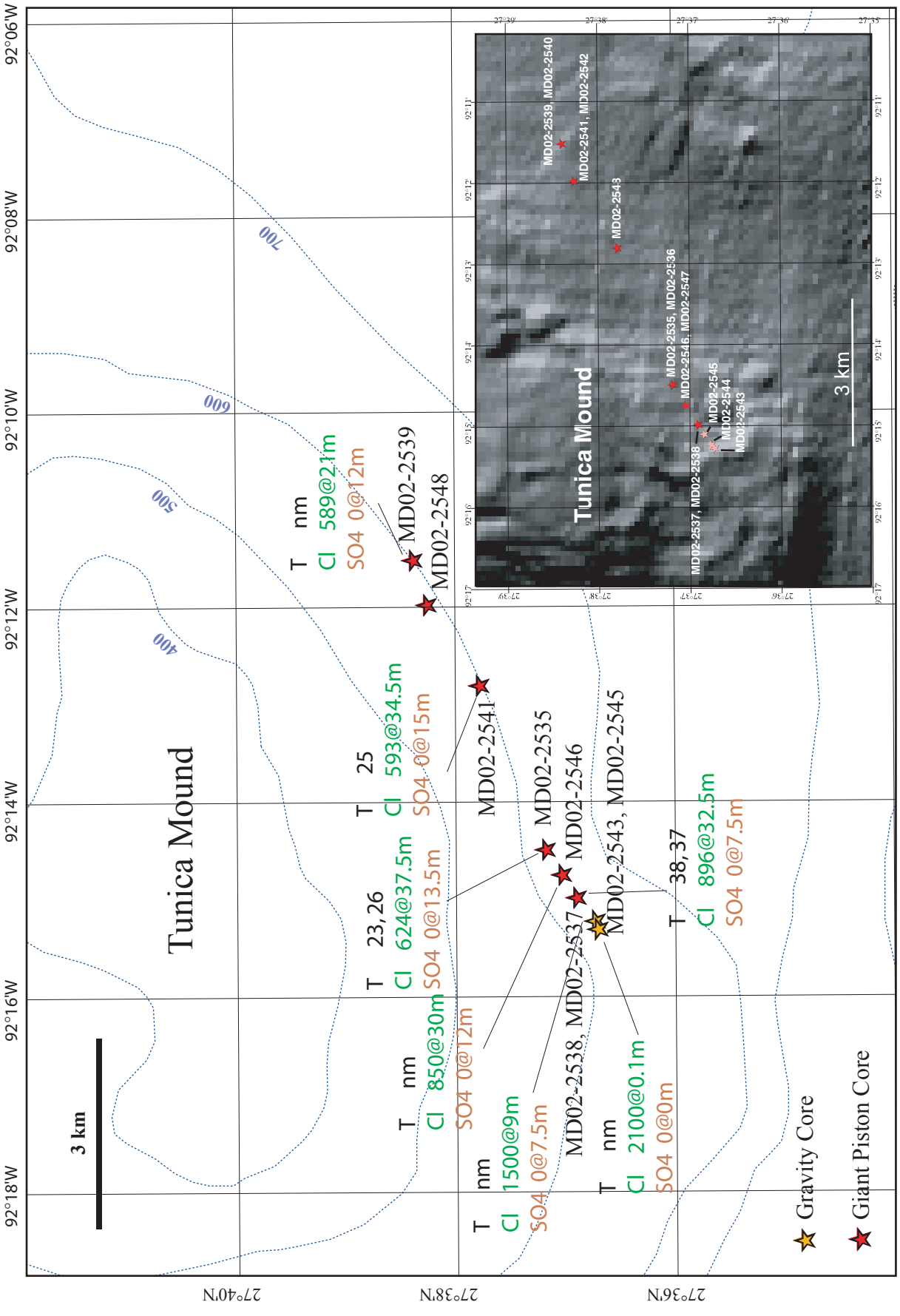

Figure 2. Core sites adjacent to Tunica Mound. Gravity and giant piston cores noted with yellow and red stars, respectively. Other core observations are indicated as follows: T = measured geothermal gradient (degrees Celsius per kilometer); Cl = chloride ion concentration (μM) maximum at the corresponding depth (meters below sea floor); SO_4 = sulfate ion concentration (μM) minimum at the corresponding depth (meters below sea floor) indicates the depth to the sulfate-methane interface (SMI); nm = not measured.

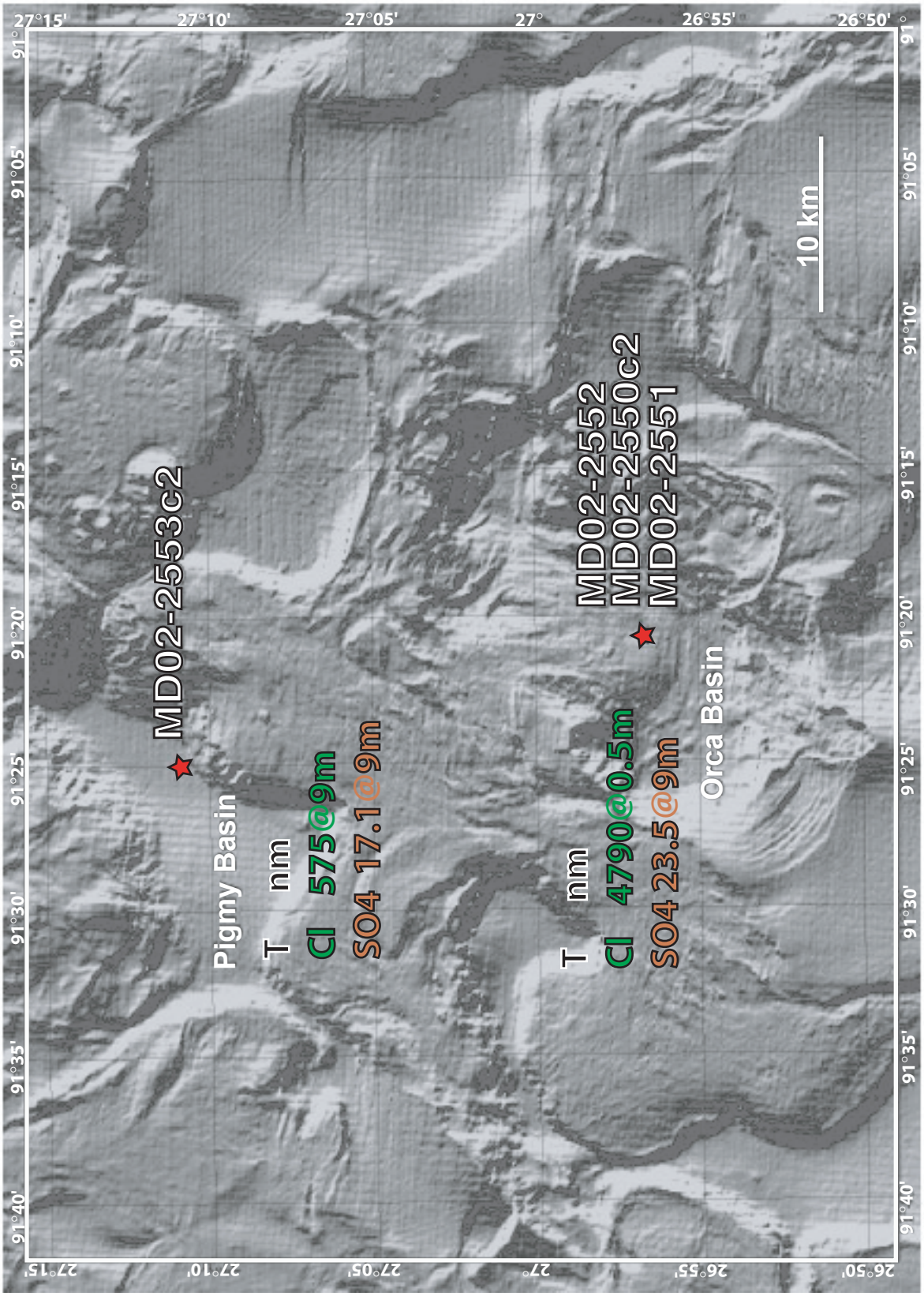

Figure 3. Core sites adjacent to Tunica Mound. Gravity and giant piston cores noted with yellow and red stars, respectively. Other core observations: T = measured geothermal gradient (nm = not measured); Cl = chloride ion concentration (μM) maximum at the corresponding depth (meters below sea floor); SO_4 = sulfate ion concentration (μM) minimum at the corresponding depth (meters below sea floor) indicates the depth to the sulfate-methane interface (SMI).

Bush Hill

The small basin just east of Bush Hill (fig. 4) was cored at a 2-kilometer (km) spacing along an east-west transect. Bush Hill itself has been extensively surveyed by numerous groups focusing on vent gas, gas hydrate, and chemosynthetic communities (MacDonald and others, 1989, 1994, 1996; Sassen and others, 1993, 1998; Roberts and Carney, 1997; Sassen, Sweet, and others 1999; Sassen, Joye, and others, 1999; Roberts, 2001; Sassen, Sweet, and others 2001a, b). The Bush Hill sea-floor feature is a fault-related seep mound at a water depth of about 540 m that may have seismic attributes of a mud diapir. An antithetic fault at Bush Hill is structurally related to nearby growth faults that constitute the structural trap at Jolliet Field just a few kilometers to the south (Cook and D'Onfro, 1991). The oil and gas at the Bush Hill site correlate with reservoirs at approximately 2 to 3 km depth in the Jolliet Field (for example, Kennicutt and others, 1988; Sassen, Losh, and others, 2001). Shallow sediment is underconsolidated hemipelagic mud with near-normal salinity (about 38 parts per thousand (ppt)), high concentration of H_2S (as much as 20.3 micromoles per liter (μM/L)), and high pH (8.3–9.0) (Aharon and Fu, 2000). Mounds of structure II gas hydrate outcrop on the sea floor and have been observed persistently since 1991 (Sassen and others, 2003).

Mississippi Canyon Region—

Kane Spur

Cooper and Hart (2003) recorded high-resolution seismic-reflection profiles across the east and west sides of the Mississippi Canyon. These areas are characterized by extreme sedimentation rates up to 15 to 20 m/k.y., with pelagic drape and mass-wasting (Coleman and others, 1983) over the last 20 thousand years (ka). The age of the sedimentary sections in the upper 600 to 700 m likely is no older than late Pleistocene age (Goodwin and Prior, 1989).

The most prominent feature on the east side of Kane Spur (fig. 5) is a large sea-floor slide that is about 15 km wide and at least 15 km long, covering more than 225 km^2. Extensional faults are found at the head of the slide, and a 1- to 2-km-wide shear zone appears along the southwest edge of the slide. The slide exhibits many features common to large-scale active slope failures in the Mississippi Canyon area resulting from several causes, including salt withdrawal and diapirism, deep- and shallow-extensional faulting, and gravity sliding (Cooper and Hart, 2003).

The subbottom is cut by two categories of faults: a suite of high-angle faults that converge with depth and extend off the bottom of the seismic-reflection record, and a set of faults that appear to be related to stratigraphic sliding within the upper sedimentary section. Cooper and Hart (2003) infer that the high-angle faults are rooted in deep-seated salt that is the principal driving mechanism for the sea-floor slide. The shallow faults that sole out within a chaotic unit partly accommodate the slide motion that includes extension near the slide's head and compression near the toe.

Within the boundaries of the extensional subsidence zone, Cooper and Hart (2003) observed a chaotic stratigraphic unit that occurs with disrupted reflections and high reflectivity. The gas hydrate stability field terminates within the high-reflectivity zone (HRZ). The top of the HRZ under the slide lies at about 440 to 480 mbsf, is about 90 to130 m thick, and generally mimics the sea floor. The high reflectivity occurs mostly where reflections are discontinuous and chaotic. The unit can be traced regionally, but reflectivity is greatest under the slide and near large fault zones. During development of the Ursa Field, drilling along the southwest side of the slide encountered wet sands with overpressured shallow water flows and some gas from about 300 to 550 mbsf (Eaton, 1999). Such features are common in the northern Gulf of Mexico (Minerals Management Service, 2001).

Mississippi Canyon Region—

MC853 Lease Block Diapiric Structure

An oblong sea-floor mound, perhaps a diapir, (1 to 1.5 km across) overlies a shallow salt body at the boundary of Mississippi Canyon lease blocks 852 and 853 referred to in this report as MC853. The MC853 sea-floor mound is on a structural high along the extensional boundary of a salt withdrawal basin on the western flank of Kane Spur (fig. 5). Allochthonous salt bodies occur at shallow depth in the sediment and have initiated major growth faults believed to serve as conduits for fluid migration to the sea floor from the subsurface petroleum system within salt withdrawal basins (Sassen, Sweet, and others, 1999). An acoustic wipeout zone typical of fluid expulsion occurs below the mound on multichannel seismic lines (Sager and Kennicutt, 2000). Intact gas hydrate has been recovered from MC 852/853 at water depths of 1,050 to 1,060 m by numerous researchers on several cruises, suggesting that the gas hydrates are persistent at the site (Sassen, Sweet, and others, 1999). Here, gas hydrate occurs within gassy sediments containing biodegraded crude oil, contains C_1–C_5 hydrocarbon gases, and is inferred to be structure II.

The estimated maximum thickness of the gas hydrate stability zone (GHSZ) is about 780 m (Appendix L). Salt is present in the near surface as evidenced by high chloride concentrations (Ussler and Paull, this volume, chapter 8). Core descriptions indicate relatively high hydrate concentration in shallow sediments with up to 90 to 100 volume percent saturation in some intervals (Sassen, Losh, and others, 2001).

Thick, relatively unfaulted sediments overlie the reservoir section of the Ursa Field. A lack of hydrocarbon seeps directly over the Ursa Field suggests that the unfaulted section is relatively impermeable. Part of the subregional fluid flow is channeled laterally along sand carrier beds out of the basin

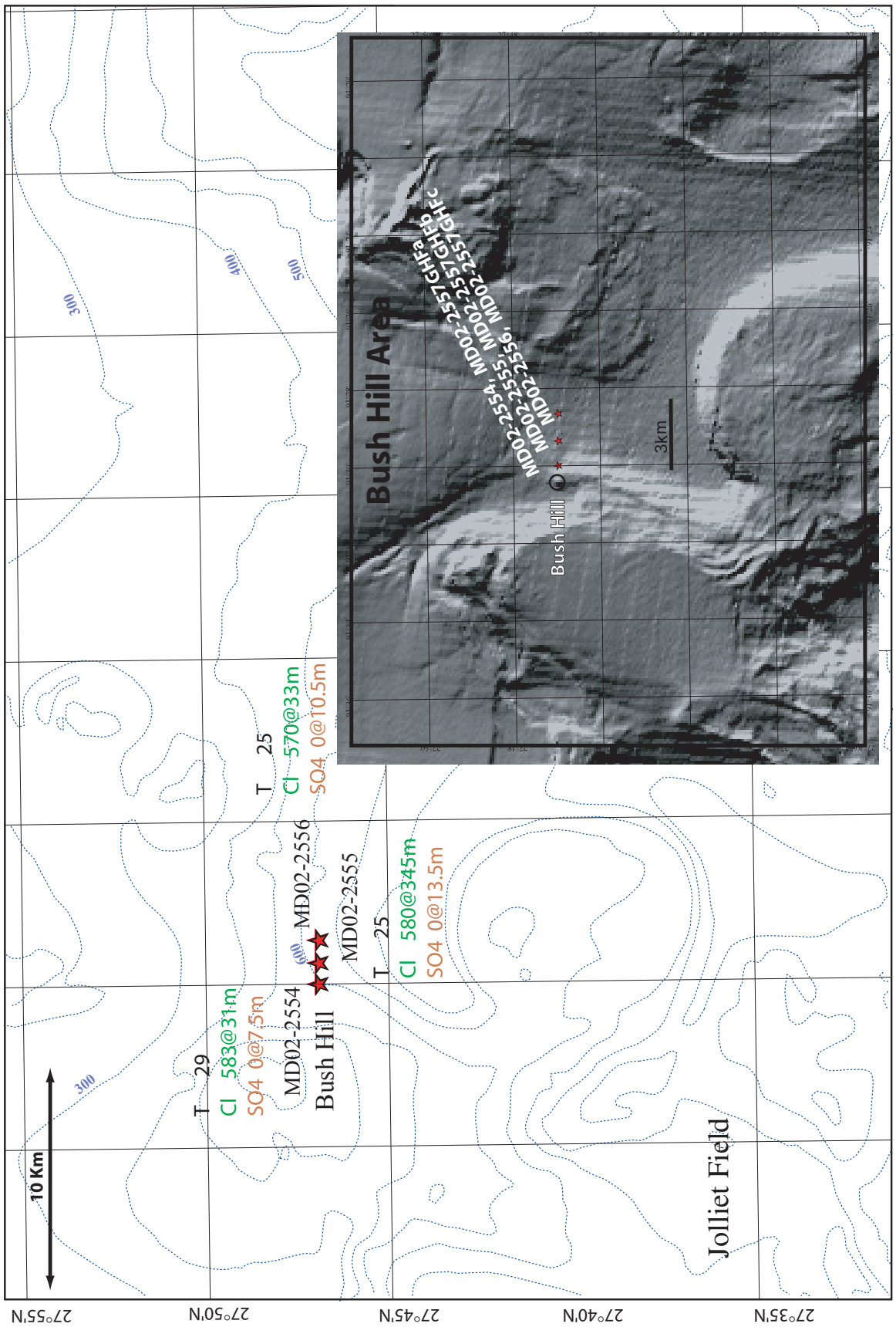

Figure 4. Giant piston core sites adjacent to Bush Hill. Core measurements: T = geothermal gradient (degrees Celsius per kilometer); Cl = chloride ion concentration (micrometers) maximum at the corresponding depth (meters below sea floor); SO_4 = sulfate ion concentration (micrometers) minimum at the corresponding depth (meters below sea floor) indicative of the depth to the sulfate-methane interface (SMI).

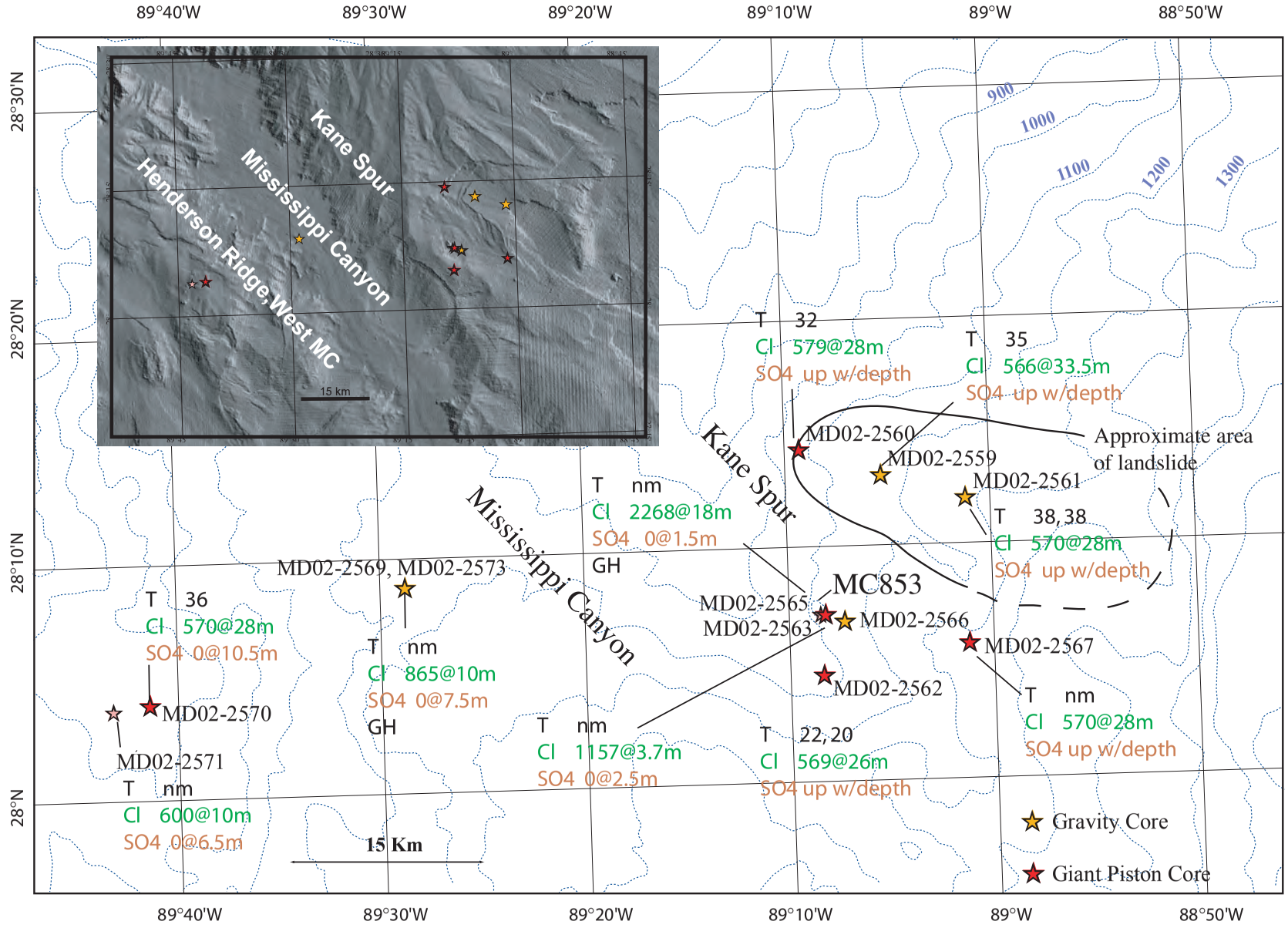

Figure 5. Core sites in the Mississippi Canyon region. Contours are in meters. Gravity and giant piston cores are noted with yellow and red stars, respectively. Core measurements: T = measured geothermal gradient (degrees Celsius per kilometer); Cl = chloride ion concentration (micrometers) maximum at the corresponding depth (meters below sea floor); SO_4 = sulfate ion concentration (micrometers) minimum at the corresponding depth (meters below sea floor) indicative of the depth to the sulfate-methane interface (SMI), up w/depth = SO_4 concentration increases with depth; nm = not measured.

to a major fluid-flow release point over the shallow salt on MC853 (Sassen, Losh, and others, 2001).

West Mississippi Canyon

West Mississippi Canyon is an area with widespread sea-floor deformation, shallow structures, and gas hydrate (fig. 5). Cooper and Hart (2003) found irregular and diffuse HRZs above diapiric structures, along high angle fault zones, laterally within layered and chaotic stratal units bounded by faults, and adjacent to acoustic wipeout zones. Gas is the likely cause of the high reflectivity; thus, localized concentrations of upward migrating gas are moving into shallow reservoirs adjacent to faults potentially forming gas hydrate. In other areas of the Gulf of Mexico's upper continental slope where acoustic wipeout zones and diffuse HRZs are seen, massive deformation, flow units, gas hydrate, and diagenetic carbonates are found within the near-sea-floor sediments (Roberts, 2001).

Results and Discussion

Sediment gas extracted from 99 samples from 23 holes was classified according to the origin of the gas (table 2): microbial (M), mainly microbial methane with some thermogenic hydrocarbons (X), and mainly thermal hydrocarbons with some microbial methane (TX). Sample depths ranged from 90 to 3,740 cm below the sea floor. Eight free-gas samples were collected and analyzed.

Tunica Mound

Gas concentrations measured on the flank of Tunica Mound (fig. 2) were highest very near the crest of a subsidiary diapir-like structure characterized by signs of active fluid flow. Methane concentrations in the nine-hole transect ranged from 24,000 μL/L in core MD02-2535 to 6 μL/L in core MD02-2538 (figs. 6–9; table 2). Methane's carbon isotopic composition ranged from –98.30 ppt PDB in core MD02-2545 to –61.20 ppt in core MD02-2543; thus, all values fall within the range expected of microbially sourced methane. Ethane and higher molecular weight hydrocarbon gas concentrations were low along the transect with the highest concentration found at a depth of about 27 m in core MD02-2535. The gas near the mound is interpreted to be from mainly microbial sources with some mixture of microbial and thermal sources (table 2). Likely input of thermogenic gases are limited to within the mound (not successfully cored because of armoring by carbonate) and very near the mound. In general, the isotopic signature of methane was found to be lighter than expected for the entire study area. Sassen and others (2003) have speculated that a deep-seated source of microbial gas exists in the north-

Table 3. Composition of hydrocarbon gas and carbon dioxide of free gas normalized to methane. Free gas was collected by drilling a hole into the core liner and inserting a syringe to collect gas.

[cm, centimeters; ppm, parts per million]

Sample ID core/depth (cm)	CO_2	C_1	C_2	C_3	iC_4	nC_4	neo-C_5	iC_5	n-C_5	c C_5	2,2MC_4	2MC_5
	ppm											
2537	6,261	993,343	360.93	7.75	0.63	0.74	3.01	0.04	0.06	0.00	0.00	0.68
2546 1600	2,259	997,076	591.85	2.33	0.64	0.64	5.02	0.00	0.00	0.02	0.00	2.24
2554 1642	8,326	991,287	352.42	4.08	0.11	0.17	2.31	0.00	0.04	0.01	0.00	1.11
2555 423	6,314	993,620	16.42	2.45	0.21	0.44	3.87	0.00	0.04	0.01	0.00	1.57
2565	24,872	919,972	24,646	23,540	3,508.43	2,524.31	31.68	560.12	123.51	37.96	16.89	34.69
2570 1500	7,072	992,217	290.34	292.62	61.86	45.38	2.96	10.68	2.43	0.43	0.25	0.66
2570 1800	5,074	994,809	84.64	6.31	0.55	0.48	1.69	0.12	0.06	0.00	0.00	0.53
2570 2000	6,099	993,769	85.89	6.01	0.44	0.00	2.96	0.00	0.00	0.00	0.00	1.97

Sample ID core/depth (cm)	3MC_5	n-C_6	McC_5	n-C_7	McC_6	C_1/C_2+C_3	iC_4/nC_4	iC_5/nC_5	C_1	CO_2	C_2	C_3
	ppm								$\delta^{13}C$	$\delta^{13}C$	$\delta^{13}C$	$\delta^{13}C$
2537	0.68	6.28	15.22	0.99	0.00	0.00	0.85	0.66	-82.19			
2546 1600	2.24	20.67	39.29	2.86	0.00	0.00	1.00		-72.24			
2554 1642	1.11	8.85	16.99	1.17	0.12	0.00	0.62	0.00	-84.24			
2555 423	1.57	13.59	25.33	2.04	0.00	0.00	0.48	0.00	-88.27			
2565	34.69	54.66	37.89	20.29	14.20	4.58	1.39	4.53	-61.83	-13.54	-29.79	-26.5
2570 1500	0.66	2.11	1.21	0.46	0.21	0.00	1.36	4.40	-70.11			
2570 1800	0.53	5.90	14.81	1.37	0.53	0.00	1.14	2.13	-70.61			
2570 2000	1.97	14.11	20.17	1.10	0.15	0.00			-70.28			

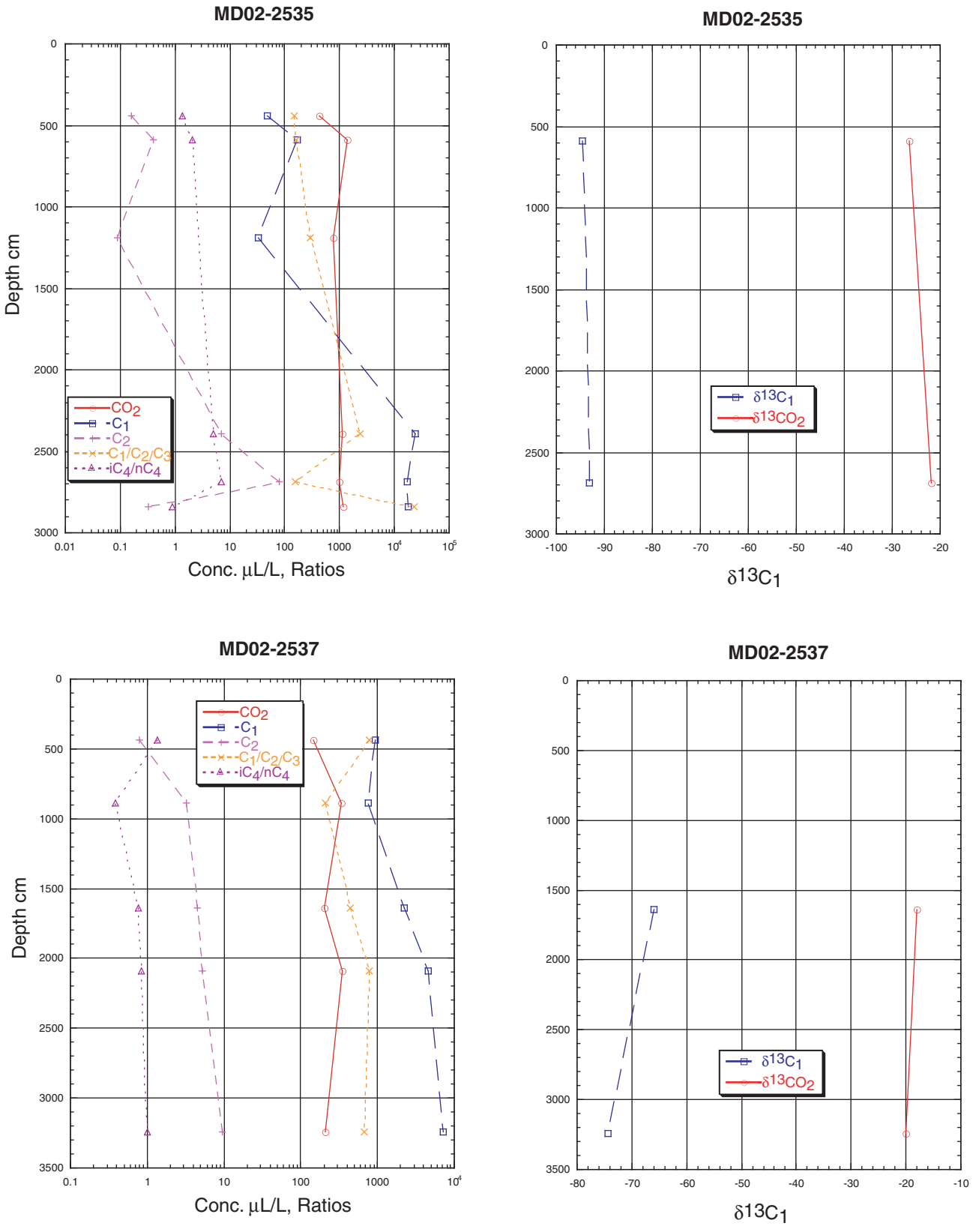

Figure 6. Plots of diagnostic sediment gas molecular composition and hydrocarbon ratios for cores MD02-2535 and MD02-2537. Core locations are shown in figure 2.

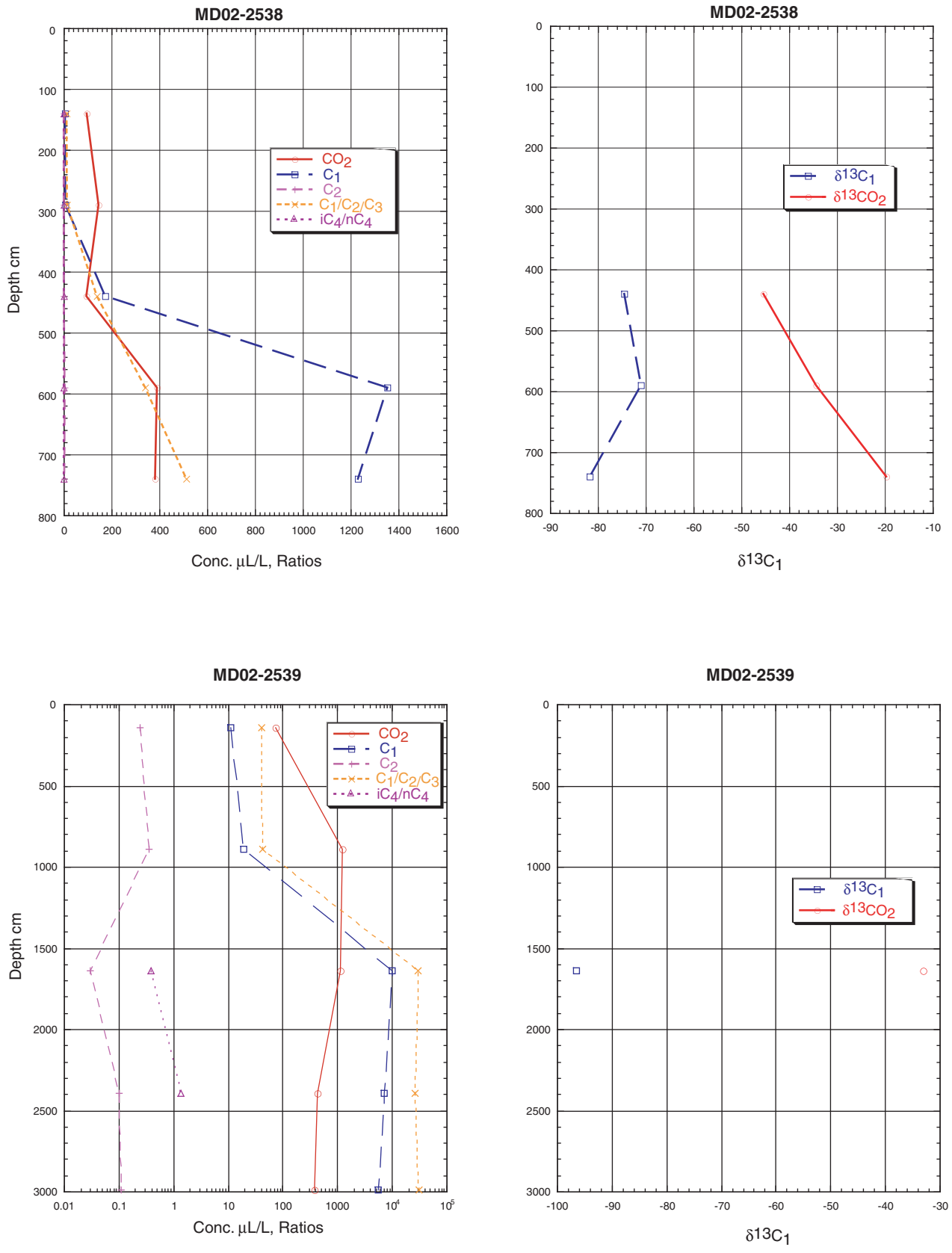

Figure 7. Plots of diagnostic sediment gas molecular composition and hydrocarbon ratios for cores MD02-2538 and MD02-2539. Core locations are shown in figure 2.

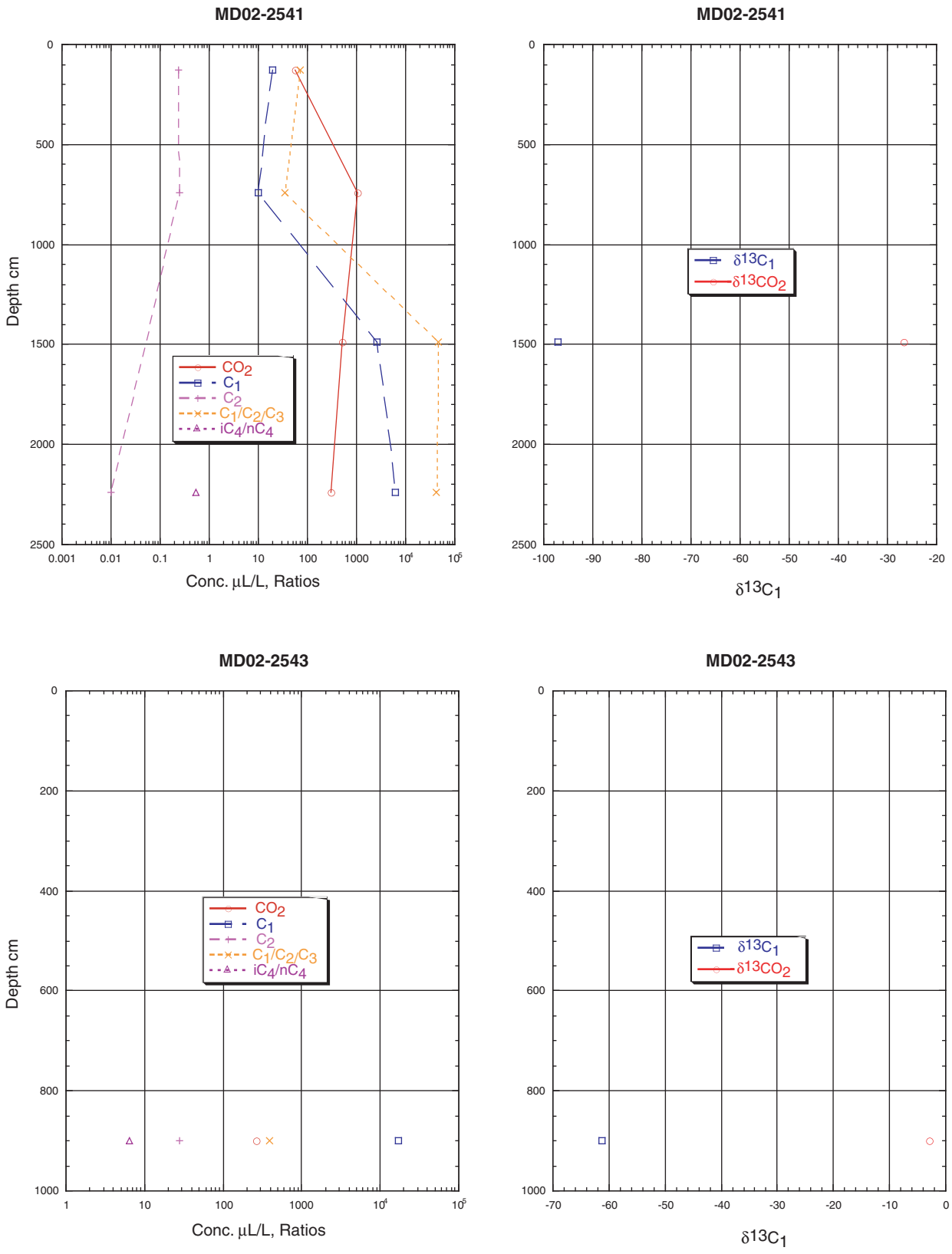

Figure 8. Plots of diagnostic sediment gas molecular composition and hydrocarbon ratios for cores MD02-2541 and MD02-2543. Core locations are shown in figure 2.

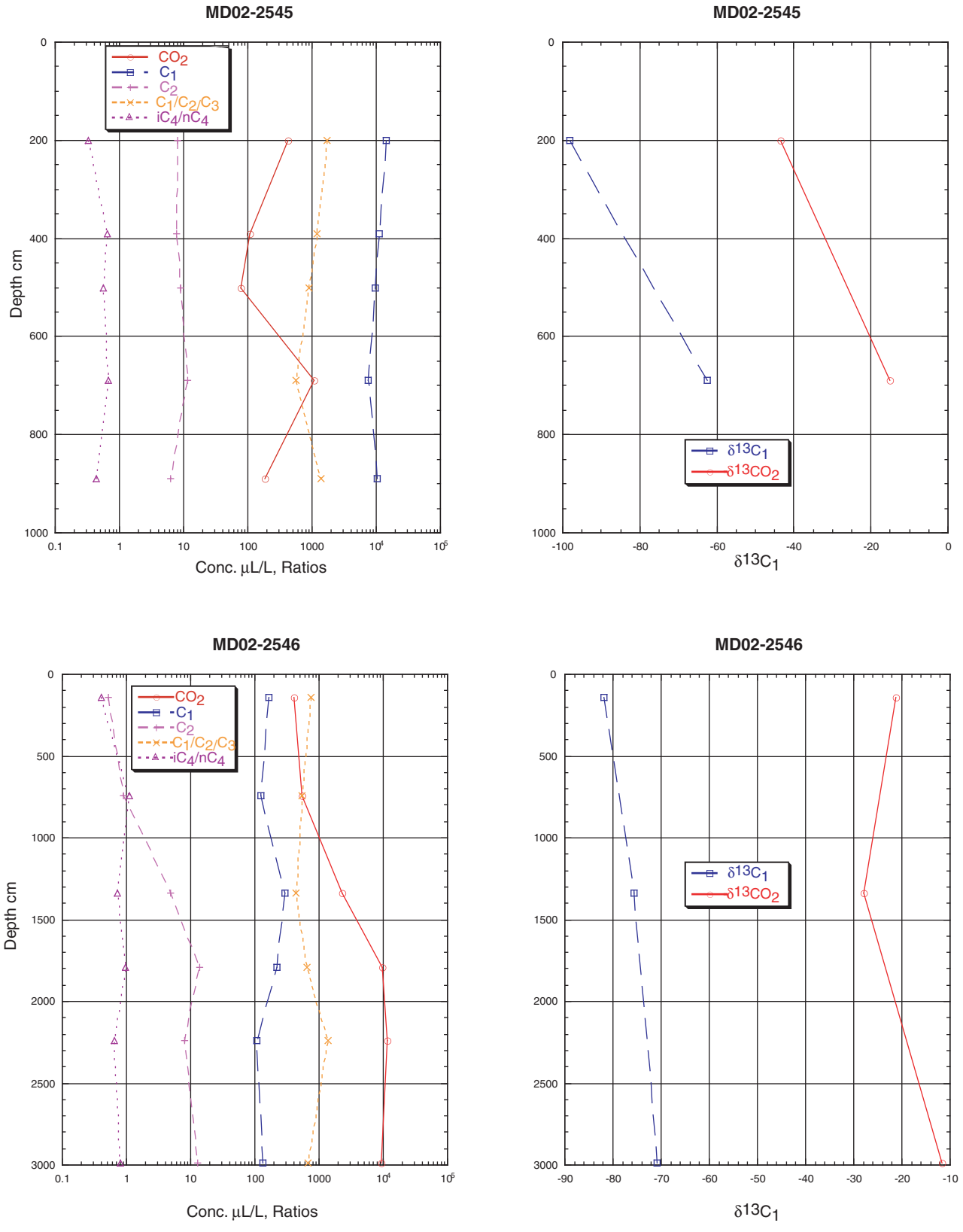

Figure 9. Plots of diagnostic sediment gas molecular composition and hydrocarbon ratios for cores MD02-2545 and MD02-2546. Core locations are shown in figure 2.

ern Gulf of Mexico, and this may be the case here and at other cored locations.

Free-gas samples were collected from cores MD02-2537 and 2546 (table 3). Gas concentrations were normalized to recovered methane values to eliminate the dilution effect of atmospheric gases that are considered artifacts of the sampling technique. Free-gas concentrations indicate that the gas is of microbial origin with greater than 99-percent methane, less than 0.1-percent ethane, and up to about 8-ppm propane. The methane is of microbial carbon isotopic composition ranging from –82.2 ppt to –72.2 ppt. The above data and the presence of high chloride concentrations (up to 2,100 mM) and shallow sulfate-methane interface (SMI, 0 to 13.5 mbsf) (Ussler and Paull, this volume, chapter 8) are consistent with fluid flow along high-angle faults flanking diapers. All indications of active fluid flow are near background levels approximately 4 km from the mound. The SMI ranges from 12 to 15 mbsf here with chloride concentrations very near those of seawater (about 560 millimoles (mM)), and the hydrocarbon gas composition is indicative of strictly a microbial source of methane.

Pigmy Basin

One gas sample was collected and analyzed from core MD02-2553 (fig. 3) within Pigmy Basin. The methane concentration was low, 136 μL/L, with a carbon isotopic composition of –45.7 and a similar carbon isotopic composition in CO_2 of –23.8‰. This thermogenic $\delta^{13}C$ coupled with a low concentration of methane indicate that the methane pool likely has been oxidized by methanotrophs (fig. 10; table 2). Higher hydrocarbons are at very low concentrations, and it is concluded that Pigmy Basin may be characterized by microbial sources of methane.

Bush Hill

Beginning on the eastern flank of Bush Hill, three cores were taken at 2-km intervals into the adjoining basin (fig. 4). Methane concentrations in the three-core transect ranged from 19,800 μL /L in core MD02-2554 to 195 μL /L in core MD02-2555 (figs. 10 and 11; table 2). The carbon isotopic composition of methane ranges from –91.1 ppt PDB in core MD02-2545 to –72.8 ppt in core MD02-2543; thus, all values fall within the isotopic range expected of microbially sourced methane. The highest concentration of ethane and higher molecular weight hydrocarbon gases were found in core MD02-2554 at a depth of about 3 m. Elsewhere, concentrations were low.

Free-gas samples were collected from cores MD02-2554 and MD02-2555 (table 3). Gases from these samples are of microbial origin with greater than 99-percent methane, less than 0.05-percent ethane, and up to about 4-ppm propane. The microbial-sourced methane has carbon isotopic composition ranging from –88.3 to –84.2 ppt.

Chloride concentrations are nearly those of seawater but increase to 583 mM in core MD02-2554, indicating the slight presence of fluid flow associated with salt dissolution. Shallow SMI's range from about 7.5 to 13.5 mbsf (Ussler and Paull, this volume, chapter 8) indicative of a substantial methane flux (Borowski and others, 1996). It is concluded that the hydrocarbon gases here are of microbial origin.

Because a number of experiments were being conducted in situ, Bush Hill itself was not cored where gas hydrate previously has been sampled. Structure II gas hydrate is abundant at Bush Hill (Sassen, Sweet, and others, 2001a) and indicates some spatial and temporal variation in composition and isotopic properties. Vein-filling gas hydrate has been discovered at Bush Hill, and this may be indicative of rapid fluid flow (Ginsburg and Soloviev, 1998). It appears that such fluid flow is bringing thermogenic hydrocarbon gases to a small venting area on the sea floor.

Two vent-gas samples collected from Bush Hill in 1998 (Sassen and others, 1998) contained thermogenic methane (90.4 to 95.9 percent) and individual C2–C5 hydrocarbons decreasing in concentration with increasing molecular weight. The $\delta^{13}C$ of this vent methane varies between –44.1 ppt and –46.0 ppt, and the δD varies between –198 ppt and –200 ppt standard mean ocean water (SMOW). The $\delta^{13}C$ of the CO_2 of the vent gas ranges from –4.9 ppt to –5.4 ppt and is consistent with a thermogenic origin of the gas. The $\delta^{13}C$ of Bush Hill gas hydrate methane had isotopic values similar to the vent gas with $\delta^{13}C$ and δD of methane at –43.6 ppt and –167 ppt, respectively, and CO_2 $\delta^{13}C$ of +17.5 ppt. Relative to the vent gases from which it likely precipitated, the gas hydrate-bound gases, including methane, occur in lower concentrations (72.1 percent), and the higher molecular-weight hydrocarbons occur in higher amounts (Sassen, Sweet, and others, 2001a).

Mississippi Canyon Region

Kane Spur

Methane concentrations in five cores ranged from 1,670 μL/L (core MD02-2559) to 6 μL/L (core MD02-2555) (figs. 12, 13, 14, and 15; table 2). The $\delta^{13}C$ of methane ranged from –93.6 ppt PDB in core MD02-2560 to –62.6 ppt in core MD02-2561, with all values falling within the isotopic range expected of microbially sourced methane. Ethane and higher molecular weight hydrocarbon gas concentrations were low in each of the five cores with the highest concentration of ethane found in core MD02-2567 (5.14 μL/L) at a depth of 13.4 m. It is concluded that the minor volumes of gas present in the upper 35 m of sediment on Kane Spur are of microbial origin.

Chloride concentrations are the same as seawater, between 566 to 579 micromoles (μM), indicative of the lack of fluid flow associated with salt dissolution within the upper 35 m of sediment. The SMI in this area is deeper than the cores and could not be penetrated. In addition, the sulfate con-

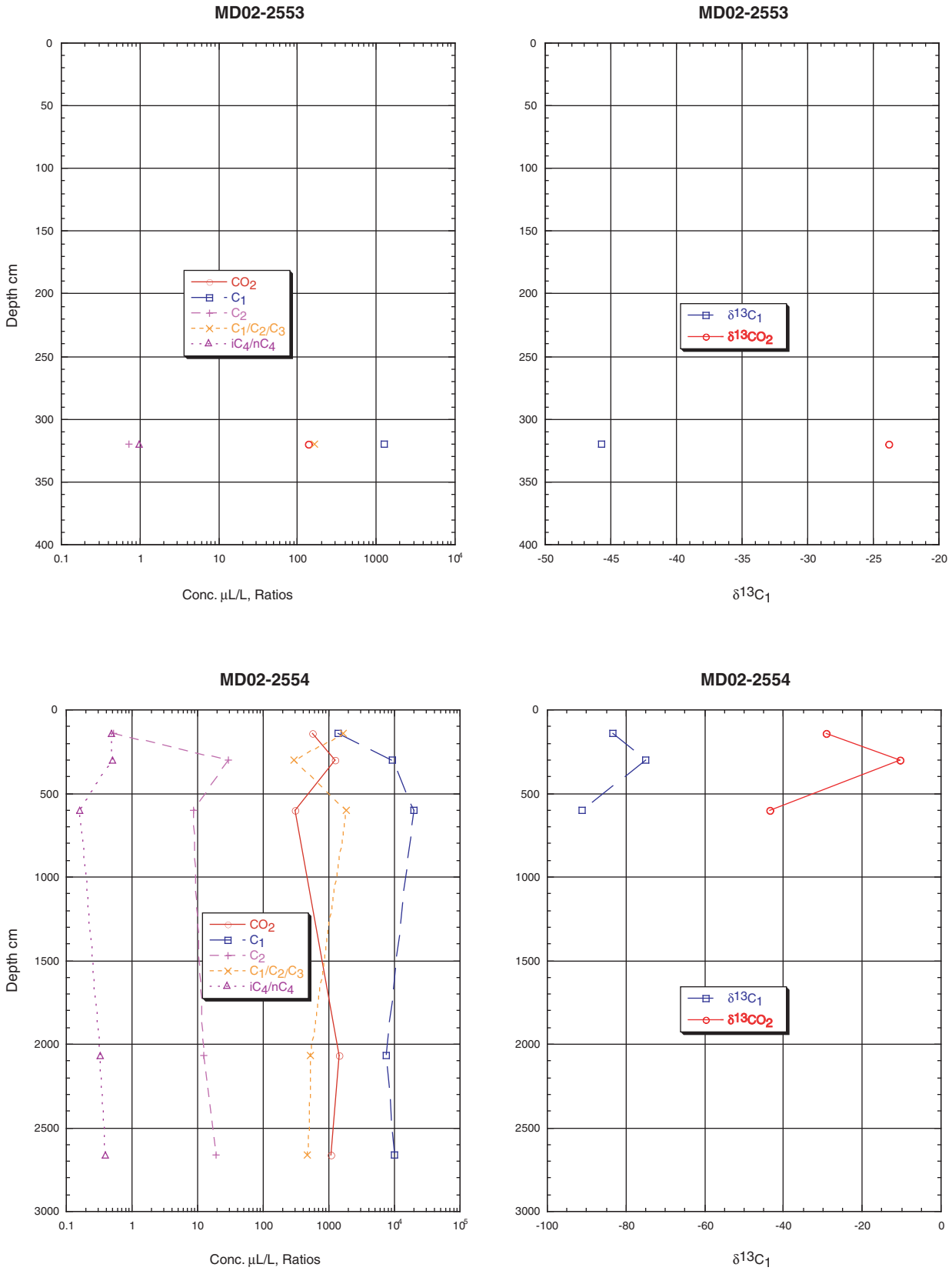

Figure 10. Plots of diagnostic sediment gas molecular composition and hydrocarbon ratios for cores MD02-2553 and MD02-2554. Core locations are shown in figures 3 and 4.

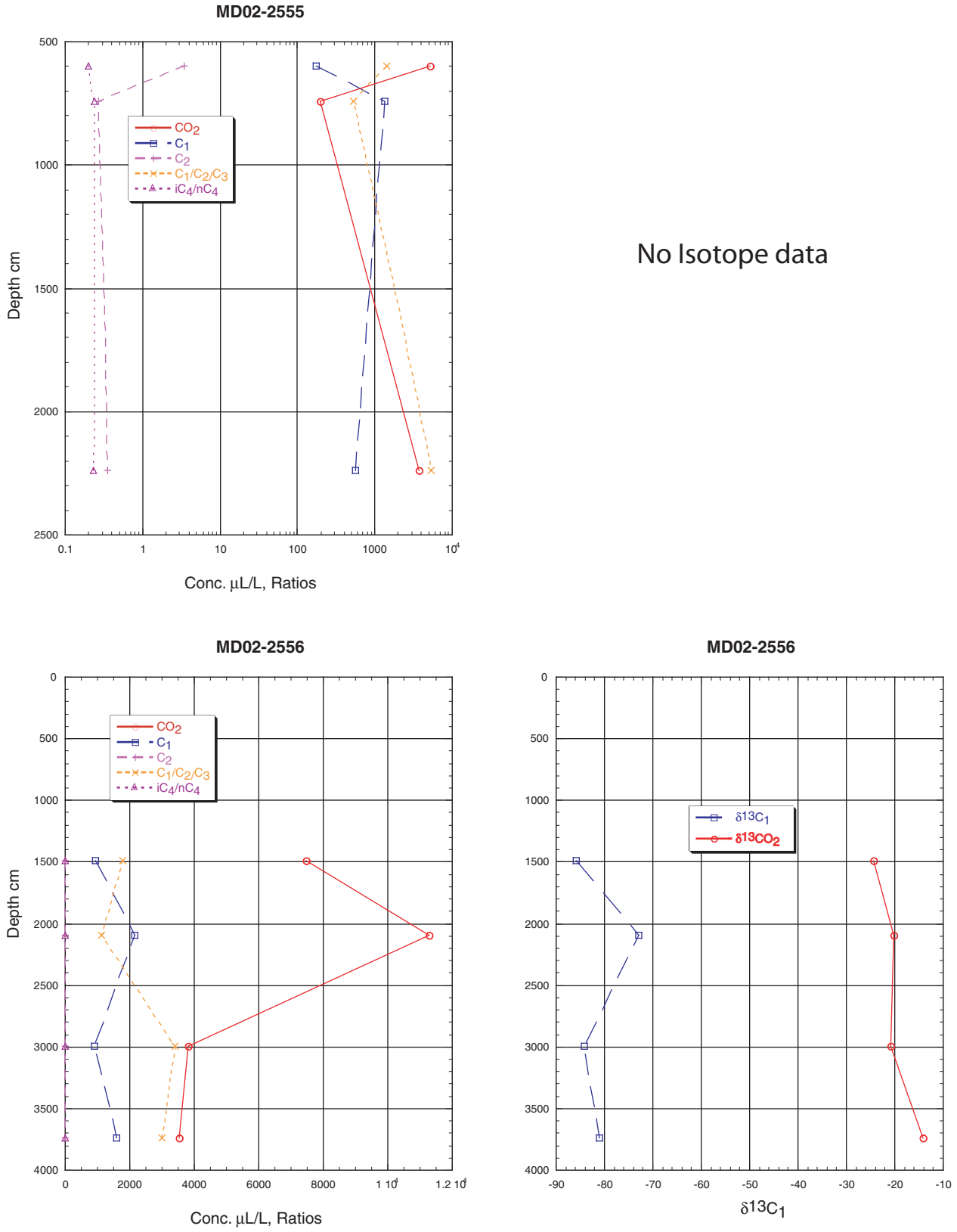

Figure 11. Plots of diagnostic sediment gas molecular composition and hydrocarbon ratios for cores MD02-2555 and MD02-2556. Core locations are shown in figure 4.

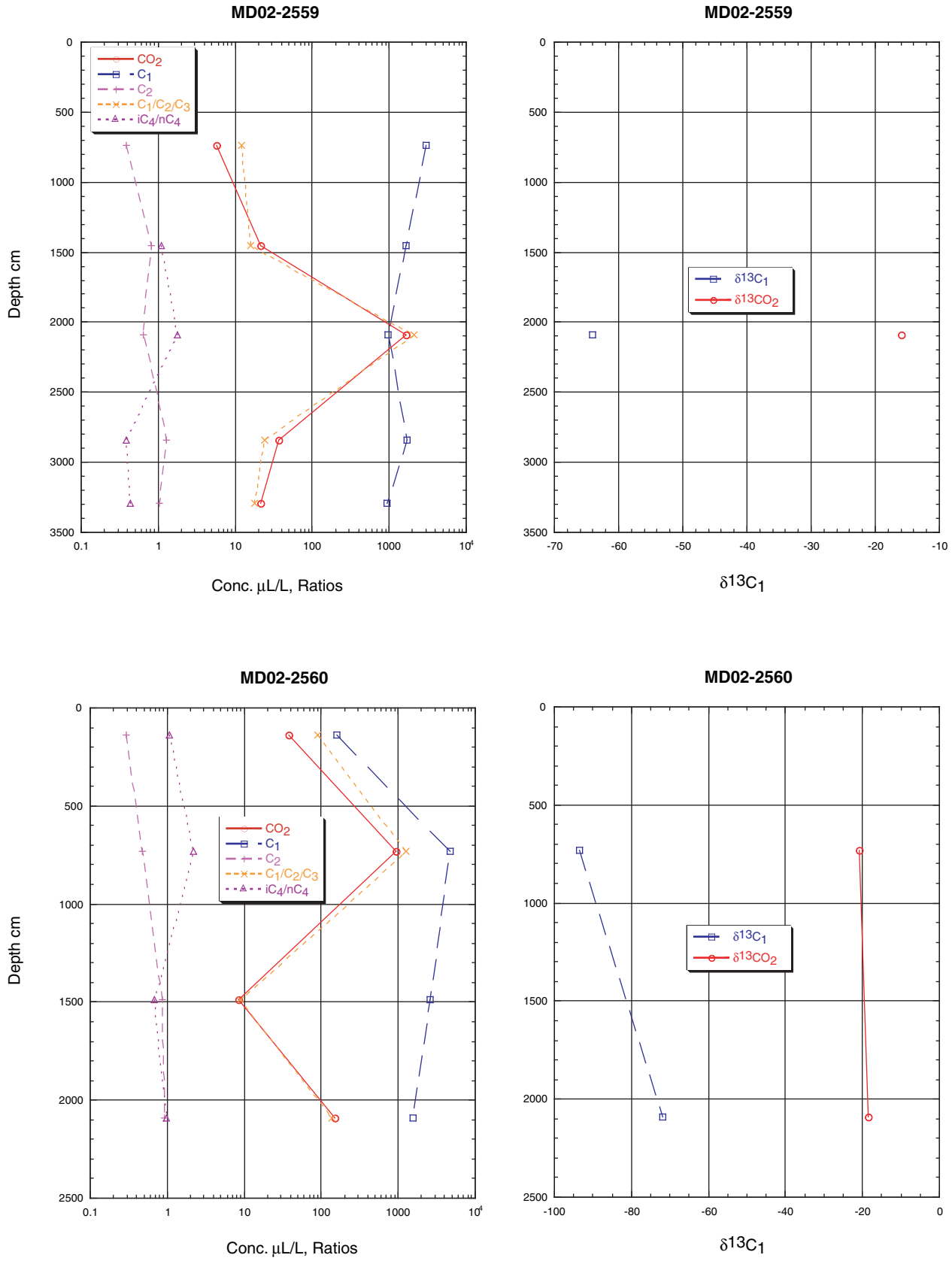

Figure 12. Plots of diagnostic sediment gas molecular composition and hydrocarbon ratios for cores MD02-2559 and MD02-2560. Core locations are shown in figure 5.

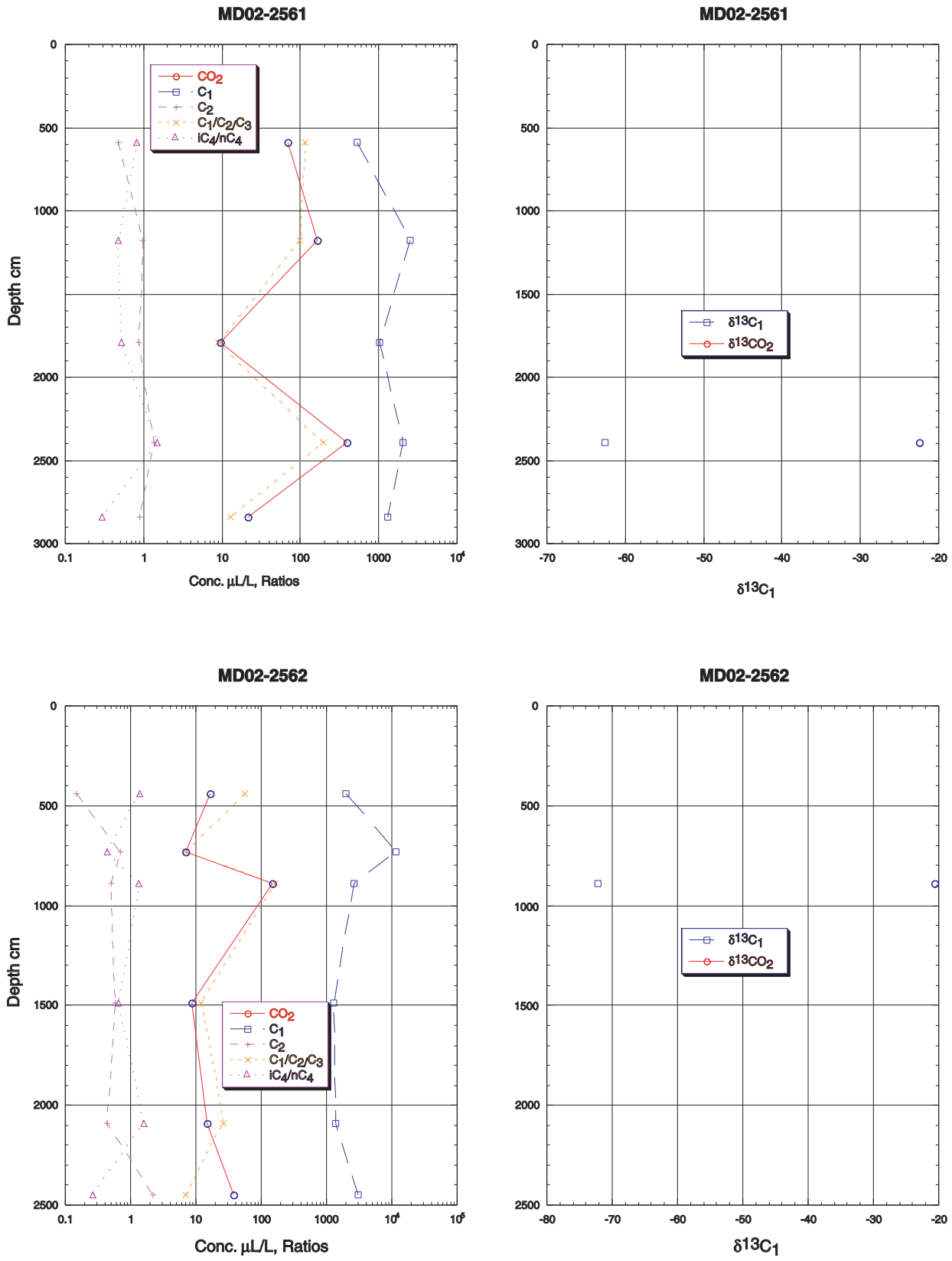

Figure 13. Plots of diagnostic sediment gas molecular composition and hydrocarbon ratios for cores MD02-2561 and MD02-2562. Core locations are shown in figure 5.

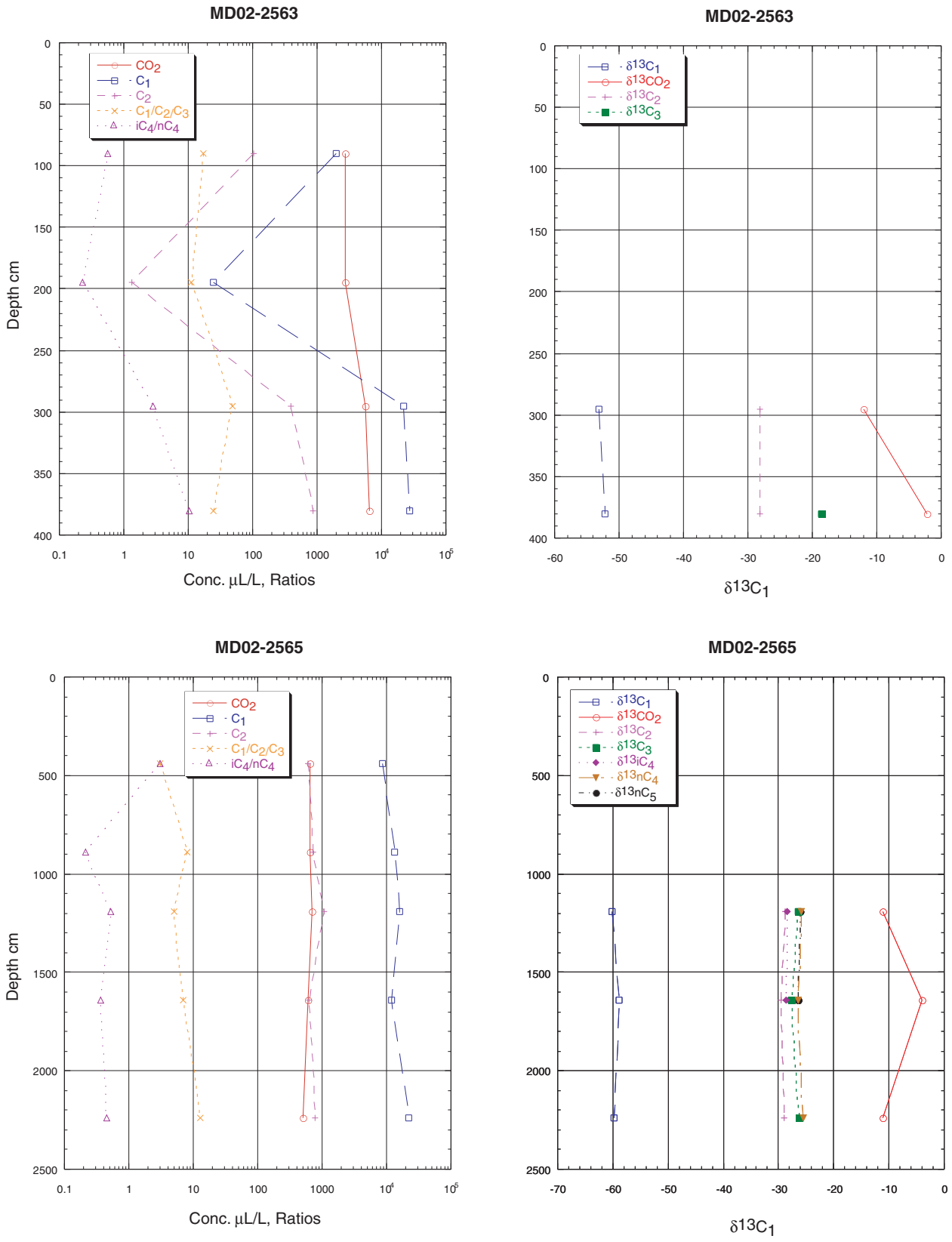

Figure 14. Plots of diagnostic sediment gas molecular composition and hydrocarbon ratios for cores MD02-2563 and MD02-2565. Core locations are shown in figure 5.

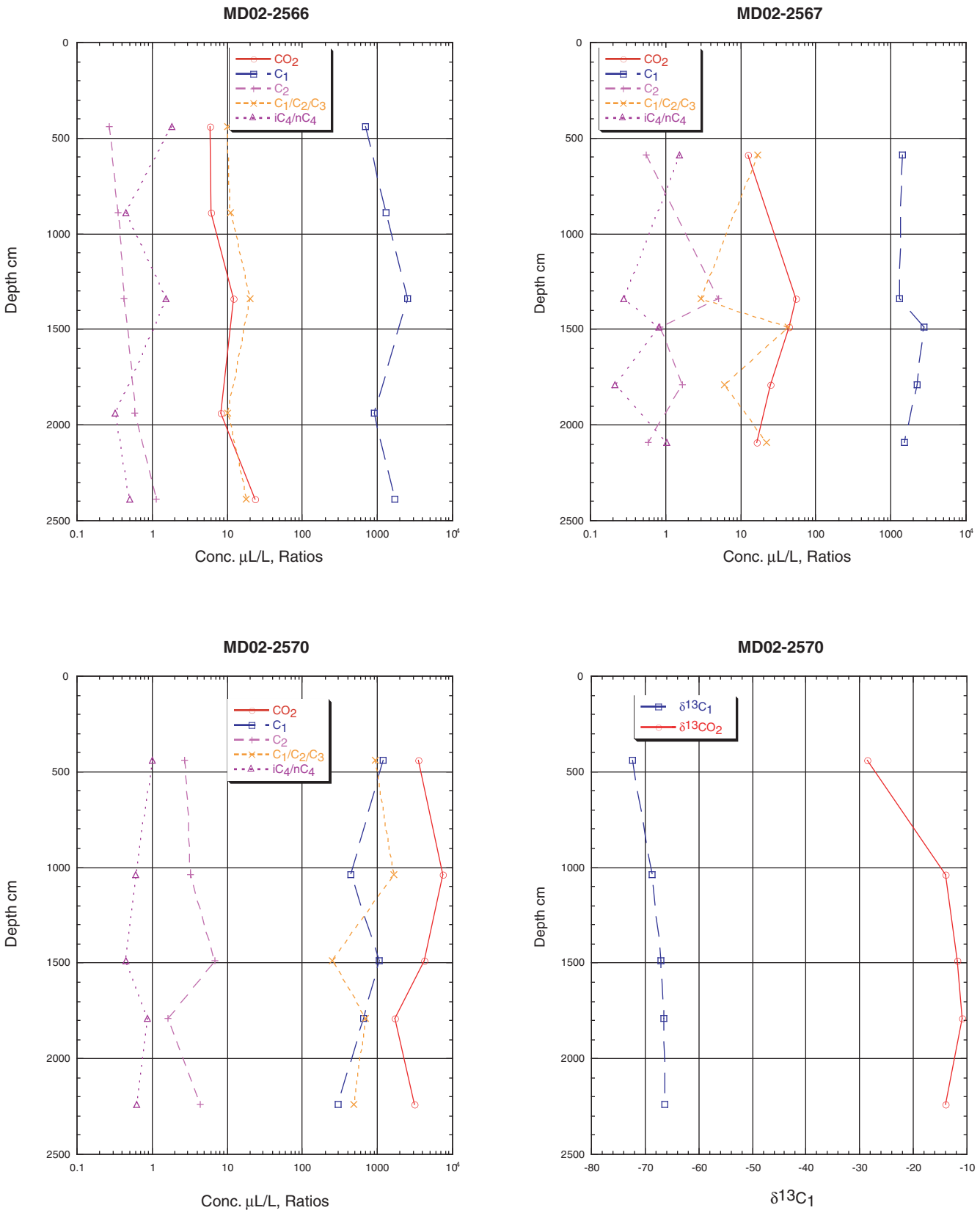

Figure 15. Plots of diagnostic sediment gas molecular composition and hydrocarbon ratios for cores MD02-2566, MD02-2567, and MD02-2570. Core locations are shown in figure 5.

centrations increase slightly with depth (Ussler and Paull, this volume, chapter 8), indicative of very little methane flux. It is concluded that the minor volumes of gas present in the upper 35 m of sediment on Kane Spur are of microbial origin.

MC853

A three-hole transect beginning near the MC853 diapir was cored. Core MD02-2566, notable for the lack of hydrocarbon gases, was taken on the southeast flank of the diapir. Two cores were taken on the summit of the diapir (MD02-2563 and MD02-2565) (fig. 5). These cores were noted for the presence of visible oil and gas of clearly thermogenic origin. Both cores contained disseminated gas hydrate, with the majority found in core MD02-2565 as indicated by over-pressuring that resulted in the upper 3 to 4 m of core exploding out of the core barrel and into the ocean. Although gas hydrate was not preserved or analyzed from this core, vigorous bubbling in the water adjacent to the ship confirmed the presence of gas hydrate (Lorenson and others, 2002).

Methane concentrations in the three-hole transect ranged from 27,300 µL/L in core MD02-2563 to 6 µL/L in core MD02-2566 (figs. 14 and 15; table 2). The $\delta^{13}C$ of methane spans from –52.2 ppt in core MD02-2563 to –60.1 ppt in core MD02-2565. These values fall within the isotopic range expected of microbially sourced methane; however, the visible presence of oil and higher molecular weight hydrocarbon gases in the core clearly confirm the presence of thermogenic hydrocarbons. Ethane and higher molecular weight hydrocarbon gas concentrations were higher near and on the diapir, with the highest ethane concentration of 1,060 µL/L found in core MD02-2565 at a depth of 12 m. The carbon isotopic composition of ethane was –28.8 ppt, indicative of a thermal origin.

In addition to ethane, higher molecular weight hydrocarbons up to normal pentane were analyzed for $\delta^{13}C$. Typically the carbon isotopic composition of hydrocarbon gas becomes heavier with increasing carbon number; however, isobutane $\delta^{13}C$ is lighter (–28.5 ppt) than propane (–27.6 ppt) or normal butane (–26.5 ppt). Typically, this result is an indication of either multiple sources or that some fractionation is occurring between the sediment gas and gas hydrate. Because there is no compelling evidence of multiple thermogenic sources of gas, the isotopic fractionation of isobutane into Structure II gas hydrate is likely. Gas hydrate gas composition from this diapir has been described previously by Sassen, Sweet, and others (1999) and by Sassen and others (2001b). Because they measured about 75-percent methane in four samples with a mean $\delta^{13}C$ of –46.6 ppt, a thermal source of methane and other hydrocarbon gases was suggested. The carbon isotopic composition of higher molecular weight hydrocarbons also showed the same trend described above for sediment gases. Thus, it is concluded that the sediment gas reflects the composition of gas hydrate here with the notable exception of methane. Methane is preferentially excluded by gas hydrate formation in favor of higher molecular weight hydrocarbons and is isotopically heavier (Sassen, Sweet, and others, 2001a).

Free gas collected from core MD02-2565 (table 3) is of mixed microbial and thermal origin. Gas measured from this core is composed of 92-percent methane, 2.5-percent ethane, 2.3-percent propane, and other higher weight hydrocarbon gases. The carbon isotopic composition of methane is –61.8 ppt, suggesting a microbial origin and indicating that there is a significant contribution of methane from microbial sources in addition to the obvious presence of thermogenic higher molecular weight hydrocarbons.

Chloride concentrations in core MD02-2566 are nearly those of seawater, indicating little fluid flow; however, the chloride concentrations are much higher (up to 2,270 µM in core MD02-2565) on the diapir, suggesting rapid fluid flow. Sulfate concentrations are higher than seawater values in core MD02-2566, similar to those on Kane Spur (Ussler and Paull, this volume, chapter 8). On the diapir, the SMI is shallow and ranges from about 1.5 to 2.5 mbsf (Ussler and Paull, this volume, chapter 8), indicative of a substantial methane flux. It is concluded that the hydrocarbon gases here are mainly thermogenic with a component of microbially sourced methane.

West Mississippi Canyon

In this region, gas chimneys and shallow faults were observed very near the sea floor by Cooper and Hart (2003) and in the thalweg of Mississippi Canyon on lease block MC802 where gas hydrate previously had been observed (Sassen and others, 1994). Gas hydrate was recovered within MC802 in cores MD02-2569 and 2573, both taken on top of the same sea-floor mound, but only in adequate amounts to obtain gas analyses from core MD02-2569. Heat-flow measurements were planned for core MD02-2573, but the core barrel was bent during recovery, making those measurements impossible. However, visible gas hydrate was found in the core-catcher. It is assumed the core met refusal at a gas hydrate layer or an authigenic carbonate layer, which caused the barrel to bend.

Methane concentrations measured in three cores from this area ranged from 19,900 µL/L (core MD02-2573) to 1,410 µL/L (core MD02-2569) (figs. 15 and 16; table 2). The methane $\delta^{13}C$ values ranged from –72.4 ppt PDB in core MD02-2570 to –59.5 ppt in core MD02-2569, therefore, all values fall within the isotopic range expected of microbially sourced methane. Ethane and higher molecular weight hydrocarbon gas concentrations generally were low with the highest ethane concentration of 70.7 µL/L found in core MD02-2573 at a depth of 2.6 m.

Three free-gas samples were collected from core MD02-2570 at depths of 15, 18, and 20 m (table 3). These samples were composed primarily of methane (99 percent) with smaller amounts of ethane (0.03 percent) and propane (300 ppm), indicating mainly a microbial origin. A modest amount of thermogenic hydrocarbons was found in the shallowest sample (15 m) while the lower samples had much less, suggesting some vertical heterogeneity or lateral gas migration

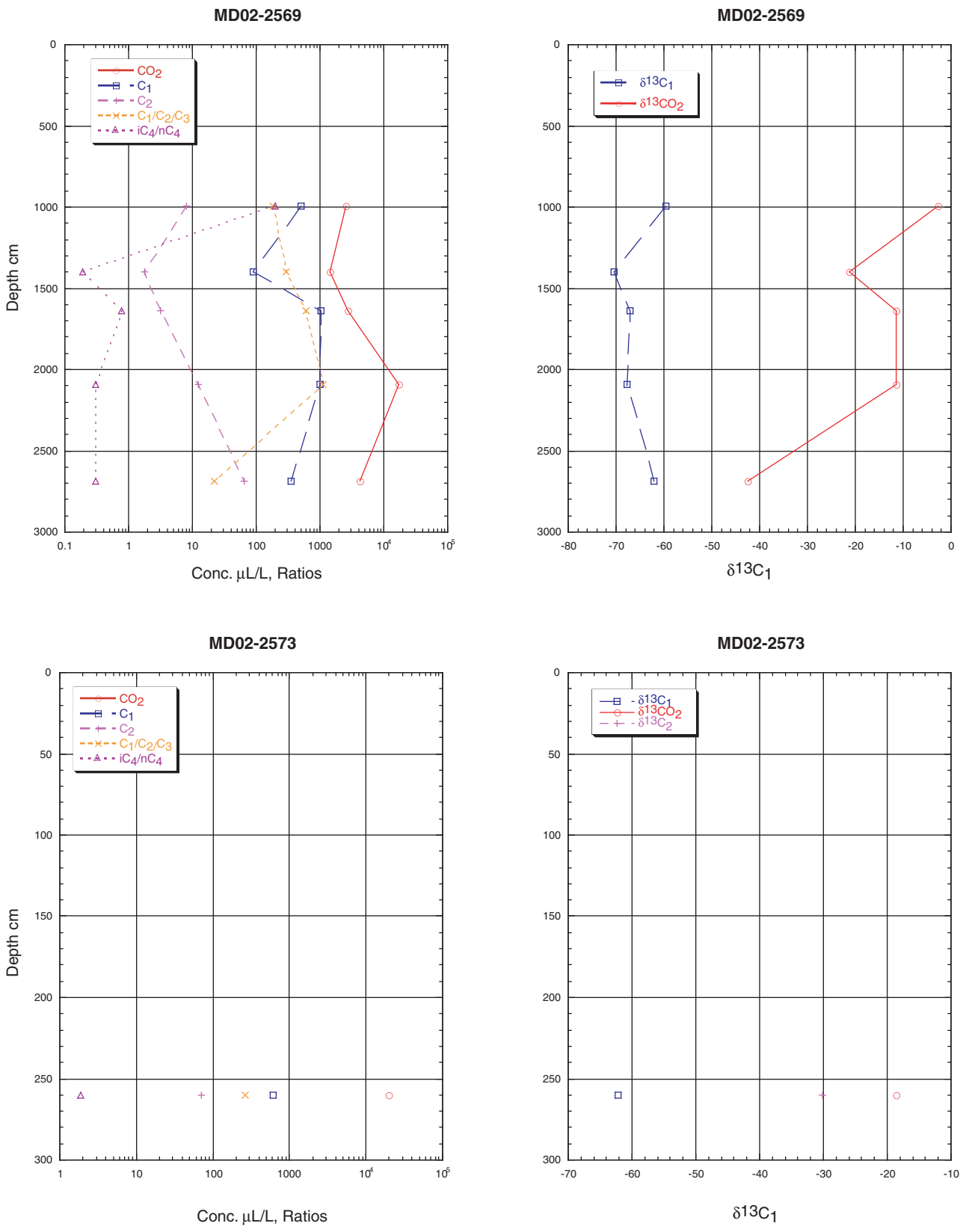

Figure 16. Plots of diagnostic sediment gas molecular composition and hydrocarbon ratios for cores MD02-2569 and MD02-2573. Core locations are shown in figure 5.

pathways. The mean $\delta^{13}C$ of methane (–70.3 ppt) suggests a microbial origin.

Lenticular bodies of gas hydrate were sampled in core MD02-2569 at two depths—3.8 and 7.0 mbsf. Results of controlled gas hydrate dissociation are presented in table 4. The quality of the gas hydrate recovered was poor because of core recovery time approaching 2 hours. Low gas-to-water ratios from dissociated samples with a maximum of 33 (170 for a fully saturated gas hydrate; Lorenson, 2000) confirmed that the samples had previously decomposed.

The composition of gas hydrate principally is methane, 95.0 to 99.5 percent, followed by CO_2 concentrations ranging from 0.16 to 4.0 percent. Higher molecular weight hydrocarbon gases—ethane, propane, and isobutane—are found in concentrations exceeding 1,000 ppm, suggesting that both structure I and structure II gas hydrate are present. The lack of normal butane suggests that gas hydrate formation here is from lean thermogenic gas (for example, the free-gas composition) selectively incorporating isobutane. A similar effect has been noted by Lorenson and others (1999) in Arctic gas hydrate accumulations.

Chloride concentrations are nearly equal to those of seawater in core MD02-2570, indicating little fluid flow associated with diapirism; however, the presence of gas and shallow faults in the seismic records (this volume, Appendix D) indicate the flow of gas without salt. Chloride concentrations are much higher (865 mM) in core MD02-2569, suggesting fluid flow associated with salt. Unpublished industry 3–D seismic records suggest the MD02-2569 site is likely a diapiric structure. The SMI is shallow and ranges from 10.5 to 7.5 mbsf (Ussler and Paull, this volume, chapter 8), indicating substantial methane flux. In conclusion, the hydrocarbon gases here are of mainly microbial origin with a component of thermogenic hydrocarbons at site MD02-2569.

Summary of Gas Origins

The majority of hydrocarbon gases encountered in this study are of microbial origin. Sassen and others (2003) have speculated that there is a deep-seated source of microbial gas in the northern Gulf of Mexico, and this observation agrees with our data.

Thermogenic gases are present in cores that are on or very near sea-floor features that exhibit active fluid venting. These areas typically are along the rims of salt withdrawal basins and

Table 4. Composition of hydrocarbon gas and carbon dioxide of gas hydrate gas normalized to methane. Gas was collected in syringes after controlled dissociation.

[ppm, parts per million; cm, centimeter; mL, milliliter]

Sample	CO_2	C_1	C_2	C_3	iC_4	nC_4	neo-C_5	iC_5	n-C_5	c C_5	2,2MC_4	2MC_5
	ppm											
2569 380 cm Vial 2	2,700	994,890	1,843.87	460.30	43.50	0.00	29.22	14.42	1.77	0.00	3.02	9.10
2569 380 cm Vial 3	40,202	949,767	7,590.37	1,079.97	1,084.72	6.42	107.47	29.03	0.00	0.00	7.33	26.31
2569 380 cm Vial 4	1,570	992,052	1,861.08	2,175.54	2,245.43	0.00	56.40	16.40	0.00	0.00	3.42	12.51
2569 700 cm Vial 3	11,407	980,376	4,093.25	1,757.19	2,208.34	0.00	61.42	12.27	0.00	0.00	2.75	10.09

Sample	3MC_5	n-C_6	McC$_5$	n-C_7	McC$_6$	Gas-to-water ratio (mL gas/mL water)	C_1/C_2+C_3	iC_4/nC_4	C_1 $\delta^{13}C$	CO_2 $\delta^{13}C$
	ppm									
2569 380 cm Vial 2	1.22	3.88	0.00	0.40	0.00	6.56	432	>1,000	-63.26	
2569 380 cm Vial 3	19.37	70.47	0.00	9.64	0.00	6.56	110	169	-62.12	-14.99
2569 380 cm Vial 4	1.85	4.27	0.00	1.74	0.00	6.56	246	>1,000	-63.11	
2569 700 cm Vial 3	8.87	51.85	0.00	11.26	0.00	33.14	168	>1,000	-54.62	

Note: Gas concentrations normalized to methane. Hydrogen and helium not measured.

active diapirism. In the northern Gulf of Mexico, this diapirism commonly is associated with saline fluids that limit the extent of the gas hydrate stability field to the near surface. Methane carbon isotopic composition in relation to the gas wetness ratio C_1/C_2+C_3 for core gas is plotted in figures 17 and 18. Primary fields representing accepted values for microbial and thermogenic sourced methane gas are noted. Most of the data fall outside these boundaries, likely reflecting mixing of microbial methane with thermogenic methane.

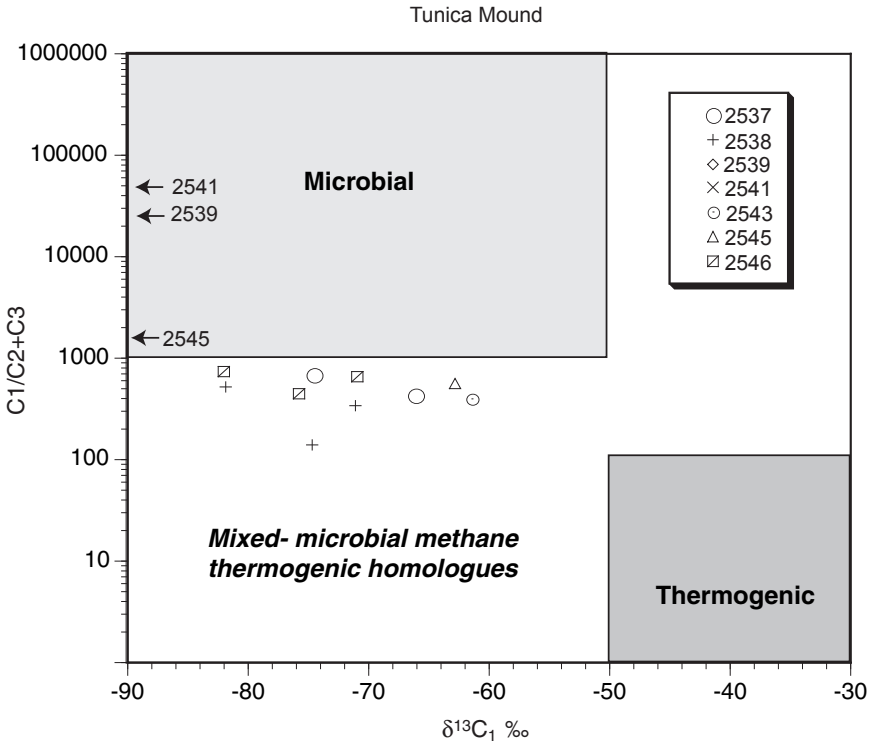

Figure 17. Plot of methane carbon isotopic composition in relation to the gas wetness ratio C_1/C_2+C_3 for Tunica Mound core gas. Primary fields representing accepted values for microbial and thermogenic-sourced methane gas are noted. Carbon isotopic compositions less than –90 are not plotted but are noted by core number with relative gas wetness ratios indicated by position on the y-axis.

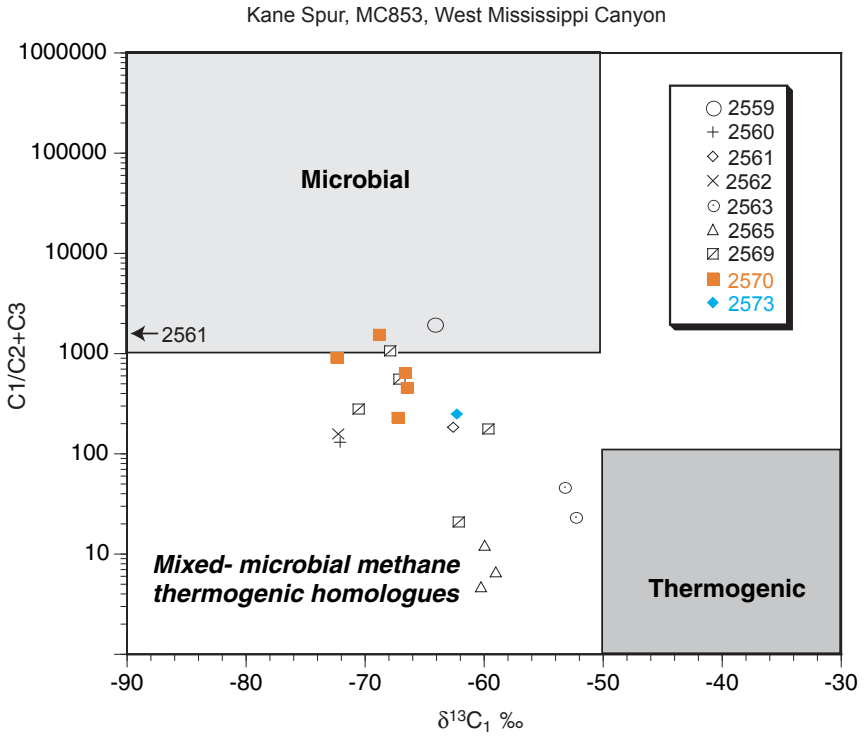

Figure 18. Plot of methane carbon isotopic composition in relation to the gas wetness ratio C_1/C_2+C_3 for Kane Spur (2559, 2560, 2561, and 2562), MC853 (2563 and 2565), and West Mississippi Canyon (2569, 2570, and 2573) core gas. Primary fields representing accepted values for microbial and thermogenic-sourced methane gas are noted. Carbon isotopic compositions less than –90 are not plotted but are noted by core number with relative gas wetness ratios indicated by position on the y-axis.

References

Aharon, P., and Fu, B., 2000, Microbial sulfate reduction rates and sulfur and oxygen isotope fractionations at oil and gas seeps in deepwater Gulf of Mexico: Geochimica et Cosmochimica Acta, v. 64, no. 2, p. 233–246.

Berryhill, H.L., Suter, J.R., and Hardin, N.S., 1987, Late Quaternary facies and structure, northern Gulf of Mexico: AAPG Studies in Geology, no. 23, 289 p.

Borowski, W.S., Paull, C.K., and Ussler, W., III, 1996, Marine pore-water sulfate profiles indicate in situ methane flux from underlying gas hydrate: Geology, v. 24, no. 7, p. 655–658.

Coleman, J.M., Prior, D.B., and Lindsay, J.F., 1983, Deltaic influences on shelf edge instability processes: SEPM Special Publication 33, p. 121–137.

Cook, D., and D'Onfro, P., 1991, Jolliet Field thrust structure and stratigraphy, Green Canyon Block 184, offshore Louisiana: Trans. —Gulf Coast Assoc. Geol. Soc., v. 41, p. 100–121.

Cooper, A.K., and Hart, P.E., 2003, High resolution seismic-reflection investigation of the northern Gulf of Mexico gas-hydrate-stability zone: Marine and Petroleum Geology, v. 19, p. 1275–1293.

Eaton, L.F., 1999, Drilling through deepwater shallow water flow zones at Ursa: Conference Proceedings Shallow Water Flows, October 6–8, 1999, Penn Well, Tulsa, OK, 600 p.

Ginsburg, G.D., and Soloviev, V.A., 1998, Submarine gas hydrates: St. Petersburg, Russia, VNII Okeangeologia, 216 p.

Goodwin, R.H., and Prior, D.B., 1989, Geometry and depositional sequences of the Mississippi Canyon, Gulf of Mexico: Journal of Sedimentary Petrologists, v. 59, no. 2, p. 318–329.

Kennicutt, M.C., II, Brooks, J.M., and Denoux, G.J., 1988, Leakage of deep, reservoired petroleum to the near surface of the Gulf of Mexico continental slope: Marine Chemistry, v. 24, p. 39–59.

Kvenvolden, K.A., Claypool, G.E., Threlkeld, C.N., and Sloan, D.E., 1984, Geochemistry of a naturally occurring massive marine gas hydrate, *in* Schenck, P.A., deLeeuw, J.W., and Lijmbach, G.W.M., eds., Advances in organic geochemistry 1983: Org. Geochem., v. 6, p. 703–713.

Kvenvolden, K.A., and Redden G.D., 1980, Hydrocarbon gas in sediment from the shelf, slope, and basin of the Bering Sea: Geochim. Cosmochim. Acta, v. 44, p. 1145–1150.

Lorenson, T.D., and Collett, T.C., 2000, Gas content and composition of gas hydrates from sediments of the southeastern North American continental margin, *in* Paull, C.K., Matsumoto, R., Wallace, P.J., and Dillon, W.P., eds., Proceedings of the Ocean Drilling Program, Scientific Results, v. 164: College Station, TX, p. 37–46.

Lorenson, T.D., Whiticar, M., Waseda, A., Dallimore, S.R., and Collett, T.S., 1999, Gas composition and isotopic geochemistry of cuttings, core, and gas hydrate from the JAPEX/JNOC/GSC Mallik 2L-38 gas hydrate research well: Geological Survey of Canada Bulletin 544, p. 143–163.

Lorenson, T.D., Winters, W., Hart, P.E., and Paull, C.K., 2002, Gas hydrate occurrence in the Northern Gulf of Mexico studied with giant piston cores: EOS, Transactions, American Geophysical Union, v. 83, no. 51 p. 601 and 607.

MacDonald, I.R., Boland, G.S., Baker, J.S., Brooks, J.M., Kennicutt, M.C., II, and Bidigare, R.R., 1989, Gulf of Mexico hydrocarbon seep communities—II. Spatial distribution of seep organisms and hydrocarbons at Bush Hill: Marine Biology, v. 101, p. 235–247.

MacDonald, I.R., Guinasso, N.L., Jr., Sassen, R., Brooks, J.M., Lee, L., and Scott, K.T., 1994, Gas hydrate that breaches the sea floor on the continental slope of the Gulf of Mexico: Geology, v. 22, p. 699–702.

MacDonald, I.R., Reilly, J.F., Jr., Best, S.E., Venkataramaiah, R., Sassen, R., Amos, J., and Guinasso, N.L., Jr., 1996, A remote-sensing inventory of active oil seeps and chemosynthetic communities in the northern Gulf of Mexico, *in* Schumacher, D., and Abrams, M.A., eds., Hydrocarbon migration and its near-surface expression: AAPG Memoir 66, p. 27–37.

Minerals Management Service, 2001, Shallow water flows in the northern Gulf of Mexico; accessed October 13, 2006, at *http://www.gomr.mms.gov/homepg/offshore/safety/wtrflow.html*

Roberts, H.H., 2001, Fluid and gas expulsion on the northern Gulf of Mexico continental slope—mud-prone to mineral-prone responses, *in* Paull, C.K., and Dillon, W.P., eds., Natural gas hydrate—occurrence, distribution, and dynamics: AGU Monograph Series, v. 24, p. 145–161.

Roberts, H.H., and Carney, R., 1997, Evidence of episodic fluid, gas and sediment venting on the northern Gulf of Mexico continental slope: Economic Geology, v. 92, p. 863–879.

Rowan, M.G., and Weimer, P., 1998, Salt-sediment interaction, northern Green Canyon and Ewing Bank (Offshore Louisiana), northern Gulf of Mexico: AAPG Bulletin, v. 82, p. 1055–1082.

Sager, W.W., and Kennicutt, M.C., 2000, Proposal for ocean drilling program research on gas hydrate in the Gulf of Mexico: Proceedings Offshore Technology Conference, 1, OTC 12111.

Sassen, R., Joye, S., Sweet, S.T., DeFreitas, D.A., Milkov, A.V., and MacDonald, I.R., 1999, Thermogenic gas hydrates and hydrocarbon gases in complex chemosynthetic communities, Gulf of Mexico continental slope: Organic Geochemistry, v. 30, p. 485–497.

Sassen, R., Losh, S.L., Cathles, L., III, Roberts, H.H., Whelan, J.K., Milkov, A.V., Sweet, S.T., and DeFreitas, D.A., 2001, Massive vein-filling gas hydrate—relation to ongoing gas migration from the deep subsurface of the Gulf of Mexico: Marine and Petroleum Geology, v. 18, no. 5, p. 551–560.

Sassen, R., MacDonald, I.R., Guinasso, N.L., Joye, S., Requejo, A.G., Sweet, S.T., Alcala-Herrera, J., DeFreitas, D.A., and Schink, D.R., 1998, Bacterial methane oxidation in sea-floor gas hydrate, Significance to life in extreme environments: Geology, v. 26, p. 289–293.

Sassen, R., MacDonald, I.R., Requejo, A.G., Guinasso, N.L., Kennicutt, M.C., II, Sweet, S.T., and Brooks, J.M., 1994, Organic geochemistry of sediments from chemosynthetic communities, Gulf of Mexico slope: Geo-Marine Letters, v. 14, p. 110–119.

Sassen, R., Milkov, A.V., Ozgul, E., Roberts, H.H., Hunt, J.L., Beeunas, M.A., and others, 2003, Gas venting and subsurface charge in the Green Canyon area, Gulf of Mexico continental slope; evidence of a deep bacterial methane source? Organic Geochemistry, v. 34, no. 10, p. 1455–1464.

Sassen, R., Roberts, H.H., Aharon, A., Larkin, J., Chinn, E.W., and Carney, R., 1993, Chemosynthetic bacterial mats at cold hydrocarbon seeps, Gulf of Mexico continental slope: Organic Geochemistry, v. 20, p. 77– 89.

Sassen, R., Sweet, S.T., Milkov, A.V., DeFreitas, D.A., and Kennicutt, M.C., II, 2001a, Thermogenic vent gas and gas hydrate in the Gulf of Mexico slope—is gas hydrate decomposition significant: Geology, v. 29, p. 107–110.

Sassen, R., Sweet, S.T., Milkov, A.V., DeFreitas, D.A., and Kennicutt, M.C., II, 2001b, Stability of thermogenic gas hydrate in the Gulf of Mexico—constraints on models of climate change, *in*, Paull, C.K., and Dillon, W.P., eds., Natural gas hydrates—occurrence, distribution, and detection: Washington, DC, American Geophysical Union, p. 131–143.

Sassen, R., Sweet, S.T., Milkov, A.V., DeFreitas, D.A., Salata, G.G., and McDade, E.C., 1999, Geology and geochemistry of gas hydrates, central Gulf of Mexico continental slope: Trans. Gulf Coast Assoc. Geol. Soc., v. 49, p. 462–468.

Weimer, P., Crews, J.R., Crow, R.S., and Varnai, P., 1998, Atlas of petroleum fields and discoveries, northern Green Canyon, Ewing Bank, and Southern Ship Shoal northern Gulf of Mexico: AAPG Bulletin, v. 82, p. 878–917.

Table 2. Composition of hydrocarbon gas and carbon dioxide of core samples.

[c, centimeter; µL/L, microliter per liter; CO_2, carbon dioxide; C_1, methane; C_2, ethane; C_3, propane; iC_4, isobutane; nC_4, normal butane; $neoC_5$, neopentane; iC_5, isopentane; nC_5, normal pentane; cC_5, cyclopentane; M, microbial; X, mainly microbial methane with some thermogenic hydrocarbons; TX, mainly thermal hydrocarbons with some microbial methane]

Core	Depth (cm)	CO_2 µL/L	C_1 µL/L	C_2 µL/L	C_3 µL/L	iC_4 µL/L	nC_4 µL/L	$neoC_5$ µL/L	iC_5 µL/L	nC_5 µL/L	cC_5 µL/L
2535	440	435	49	0.16	0.17	0.14	0.10	0.00	0.09	0.11	0.00
2535	590	1,404	166	0.40	0.61	0.53	0.25	0.00	0.20	0.06	0.24
2535	1,190	774	33	0.09	0.02	0.00	0.00	0.00	0.00	0.18	0.00
2535	2,,390	1,115	23,847	6.97	3.07	1.33	0.27	4.43	0.36	0.06	0.30
2535	2690	1,004	17,240	80.57	31.19	9.32	1.31	42.04	1.23	0.00	0.00
2535	2,840	1,191	17,750	0.33	0.43	0.16	0.18	0.04	0.10	0.06	0.16
2537	440	144	938	0.80	0.41	0.23	0.17	0.02	0.13	0.06	0.26
2537	890	337	748	3.20	0.34	0.02	0.05	0.00	0.01	0.00	0.00
2537	1,640	205	2,242	4.56	0.57	0.14	0.19	0.11	0.29	0.08	0.31
2537	2,090	350	4,587	5.29	0.57	0.18	0.22	0.02	0.11	0.05	0.14
2537	3,240	209	7,089	9.49	0.96	0.34	0.33	0.03	0.40	0.09	0.34
2538	140	96	6	0.39	0.07	0.00	0.01	0.02	0.01	0.00	0.00
2538	290	145	7	0.43	0.07	0.06	0.06	0.07	0.17	0.07	0.21
2538	440	94	174	0.51	0.75	0.71	0.50	0.02	0.40	0.16	0.62
2538	590	390	1,353	3.73	0.24	0.01	0.04	0.02	0.01	0.01	0.00
2538	740	382	1,231	2.19	0.21	0.02	0.06	0.02	0.02	0.00	0.00
2539	140	75	11	0.24	0.04	0.00	0.00	0.00	0.00	0.00	0.00
2539	890	1,221	19	0.36	0.08	0.00	0.02	0.01	0.00	0.00	0.00
2539	1,640	1,130	10,105	0.03	0.30	0.02	0.05	0.01	0.00	0.00	0.00
2539	2,390	431	7,233	0.10	0.18	0.17	0.12	0.13	0.34	0.11	0.43
2539	2,990	381	5,434	0.11	0.07	0.00	0.02	0.01	0.01	0.00	0.00
2541	130	56	20	0.24	0.03	0.01	0.00	0.02	0.04	0.00	0.05
2541	740	1,027	10	0.25	0.04	0.00	0.01	0.01	0.00	0.00	0.00
2541	1,490	504	2,637	0.00	0.06	0.00	0.02	0.01	0.01	0.00	0.00
2541	2,240	298	6,107	0.01	0.13	0.03	0.05	0.04	0.09	0.04	0.11
2543	900	266	16,881	27.60	15.15	8.82	1.39	3.49	2.40	0.11	0.20
2545	200	419	14,481	8.19	0.40	0.02	0.06	0.03	0.01	0.01	0.00
2545	390	109	10,943	7.81	1.39	0.18	0.27	0.04	0.04	0.01	0.00
2545	500	77	9,581	9.07	1.49	0.17	0.30	0.06	0.05	0.01	0.00
2545	690	1,072	7,444	11.45	1.76	0.23	0.34	0.14	0.23	0.05	0.21
2545	890	186	10,353	6.28	1.22	0.12	0.27	0.18	0.07	0.02	0.00
2546	140	167	404	0.52	0.02	0.01	0.01	0.01	0.03	0.01	0.02
2546	740	124	551	0.90	0.12	0.07	0.06	0.06	0.17	0.04	0.17
2546	1,340	291	2,277	4.92	0.27	0.05	0.07	0.00	0.02	0.01	0.00
2546	1,790	220	9,625	14.07	0.63	0.29	0.29	0.11	0.27	0.08	0.25
2546	2,240	107	11,391	8.01	0.30	0.07	0.12	0.02	0.04	0.02	0.00

Table 2. Composition of hydrocarbon gas and carbon dioxide of core samples. — Continued

[c, centimeter; µL/L, microliter per liter; CO_2, carbon dioxide; C_1, methane; C_2, ethane; C_3, propane; iC_4, isobutane; nC_4, normal butane; $neoC_5$, neopentane; iC_5, isopentane; nC_5, normal pentane; cC_5, cyclopentane; M, microbial; X, mainly microbial methane with some thermogenic hydrocarbons; TX, mainly thermal hydrocarbons with some microbial methane]

Core	Depth (cm)	CO_2 µL/L	C_1 µL/L	C_2 µL/L	C_3 µL/L	iC_4 µL/L	nC_4 µL/L	$neoC_5$ µL/L	iC_5 µL/L	nC_5 µL/L	cC_5 µL/L
2546	2,990	131	9,308	12.65	1.27	0.21	0.26	0.07	0.14	0.04	0.00
2553	2,814	1,246	136	0.72	0.10	0.04	0.04	0.01	0.03	0.10	0.03
2554	140	556	1,386	0.53	0.29	0.16	0.34	0.05	0.20	0.18	0.10
2554	300	1,241	9,399	29.09	2.88	0.12	0.24	0.02	0.05	0.00	0.00
2554	600	309	19,750	8.70	2.10	0.02	0.10	0.03	0.02	0.02	0.00
2554	2,065	1,437	7,574	12.39	1.98	0.39	1.21	0.05	0.91	0.47	0.20
2554	2,665	1,061	10,081	19.30	1.89	0.08	0.19	0.02	0.04	0.02	0.00
2555	600	177	5,148	3.42	0.17	0.02	0.08	0.04	0.01	0.01	0.00
2555	740	1,353	195	0.27	0.10	0.01	0.03	0.03	0.01	0.01	0.00
2555	2,240	556	3,690	0.35	0.34	0.02	0.09	0.01	0.01	0.01	0.00
2556	1,490	923	7,476	3.42	0.81	0.39	0.89	2.74	0.67	0.28	0.15
2556	2,090	2,143	11,283	2.05	7.99	1.78	9.45	0.06	5.04	2.51	0.62
2556	2,990	894	3,818	0.40	0.72	0.12	0.35	0.03	0.16	0.00	0.10
2556	3,740	1,587	3,535	0.38	0.80	0.13	0.23	0.03	0.07	0.00	0.07
2559	740	3,043	6	0.39	0.09	0.00	0.03	0.05	0.01	0.80	0.00
2559	1,450	1,660	21	0.82	0.55	0.46	0.42	0.03	0.39	0.21	0.00
2559	2,090	977	1,673	0.64	0.16	0.18	0.10	0.00	0.07	0.05	0.12
2559	2,840	1,681	37	1.26	0.27	0.14	0.36	0.03	0.33	0.12	0.08
2559	3,290	948	21	1.03	0.18	0.06	0.14	0.02	0.12	0.05	0.03
2560	140	158	38	0.29	0.14	0.07	0.07	0.03	0.08	0.03	0.07
2560	730	4,742	944	0.47	0.27	0.23	0.10	0.00	0.06	0.03	0.00
2560	1,490	2,611	8	0.87	0.10	0.02	0.02	0.03	0.02	0.05	0.00
2560	2,090	1,543	150	0.92	0.16	0.08	0.08	0.02	0.09	0.03	0.08
2561	590	525	68	0.47	0.12	0.03	0.03	0.00	0.01	0.03	0.00
2561	1,180	2,555	166	0.99	0.67	0.33	0.70	0.49	0.35	0.30	0.16
2561	1,790	1,017	9	0.87	0.21	0.13	0.26	0.02	0.11	0.02	0.05
2561	2,390	2,067	393	1.37	0.64	0.56	0.37	0.02	0.29	0.10	0.00
2561	2,840	1,311	22	0.89	0.73	0.26	0.89	0.04	0.75	0.37	0.16
2562	440	1,959	17	0.15	0.15	0.11	0.08	0.00	0.06	0.00	0.09
2562	730	11,387	7	0.71	0.23	0.09	0.20	0.05	0.21	0.09	0.07
2562	890	2,596	147	0.51	0.38	0.29	0.22	0.02	0.14	0.05	0.18
2562	1,490	1,280	9	0.59	0.13	0.08	0.11	0.02	0.11	0.05	0.06
2562	2,090	1,376	15	0.44	0.13	0.11	0.07	0.01	0.05	0.01	0.06
2562	2,450	3,082	37	2.21	3.25	1.42	5.52	0.02	2.76	3.54	0.00
2563	90	2,695	1,976	104.48	13.65	2.37	4.14	11.65	3.63	1.92	0.27

Table 2. Composition of hydrocarbon gas and carbon dioxide of core samples. — Continued

[c, centimeter; µL/L, microliter per liter; CO_2, carbon dioxide; C_1, methane; C_2, ethane; C_3, propane; iC_4, isobutane; nC_4, normal butane; $neoC_5$, neopentane; iC_5, isopentane; nC_5, normal pentane; cC_5, cyclopentane; M, microbial; X, mainly microbial methane with some thermogenic hydrocarbons; TX, mainly thermal hydrocarbons with some microbial methane]

Core	Depth (cm)	CO_2 µL/L	C_1 µL/L	C_2 µL/L	C_3 µL/L	iC_4 µL/L	nC_4 µL/L	$neoC_5$ µL/L	iC_5 µL/L	nC_5 µL/L	cC_5 µL/L
2563	295	5,530	22,293	393.82	56.87	21.15	7.58	164.83	5.24	0.79	0.05
2563	380	6,460	27,274	858.40	247.02	107.69	10.41	409.68	13.17	0.62	4.35
2565	440	653	8,719	615.00	2322.47	1,995.15	655.05	22.44	413.87	87.31	227.44
2565	890	651	13,464	710.72	914.68	281.99	1,359.92	3.74	1,041.04	245.11	26.80
2565	1,190	708	16,191	1057.77	2038.86	602.47	1,150.62	8.41	445.62	238.69	54.40
2565	1,640	595	12,137	633.55	1175.73	383.08	1,066.64	3.70	417.06	254.99	30.38
2565	2,240	501	22,370	773.56	1006.22	28.86	62.15	1.78	196.04	153.67	29.53
2566	440	702	6	0.27	0.30	0.27	0.14	0.01	0.12	0.09	0.20
2566	890	1,300	6	0.35	0.18	0.08	0.18	0.02	0.09	0.12	0.04
2566	1,340	2,481	12	0.42	0.19	0.16	0.10	0.01	0.08	0.06	0.12
2566	1,940	898	8	0.58	0.21	0.08	0.24	0.00	0.11	0.02	0.05
2566	2,390	1,702	23	1.13	0.16	0.08	0.16	0.03	0.10	0.03	0.06
2567	590	1,413	12	0.55	0.17	0.17	0.11	0.01	0.09	0.05	0.15
2567	1,340	1,297	55	5.14	12.77	5.18	18.34	0.04	8.09	8.69	0.00
2567	1,490	2,766	44	0.84	0.18	0.13	0.16	0.00	0.10	0.02	0.06
2567	1,790	2,208	25	1.70	2.33	0.79	3.73	0.02	1.85	2.36	0.50
2567	2,090	1,535	16	0.58	0.15	0.09	0.09	0.02	0.12	0.01	0.09
2569	995	504	2,589	8.14	5.90	10.48	0.05	4.19	0.74	0.13	0.00
2569	1,400	89	1,412	1.77	3.01	0.91	4.84	0.10	3.27	2.02	0.24
2569	1,640	1,029	2,692	3.16	1.34	0.33	0.43	0.76	0.16	0.12	0.00
2569	2,090	997	17,223	12.31	3.21	0.41	1.31	0.48	0.91	0.50	0.19
2569	2,690	347	4,191	65.10	129.30	34.71	114.95	1.16	37.60	19.77	2.07
2570	440	1,177	3,507	2.67	1.02	0.50	0.50	0.05	0.30	0.14	0.00
2570	1,040	447	7,441	3.27	1.26	0.39	0.63	0.08	0.27	0.38	0.00
2570	1,490	1,056	4,197	6.89	9.94	3.01	6.75	0.36	5.01	1.90	0.55
2570	1,790	660	1,727	1.63	0.85	0.11	0.13	0.38	0.07	0.10	0.00
2570	2,240	295	3,116	4.38	2.12	0.56	0.90	0.33	0.72	0.30	0.15
2573	260	611	19,870	70.66	5.37	2.56	1.37	55.16	2.21	0.55	0.17

Table 2. Composition of hydrocarbon gas and carbon dioxide of core samples. — Continued

[c, centimeter; µL/L, microliter per liter; M, microbial; X, mainly microbial methane with some thermogenic hydrocarbons; TX, mainly thermal hydrocarbons with some microbial methane]

Core	Depth (cm)	2,2MC$_4$ µL/L	2MC$_5$ µL/L	3MC$_5$ µL/L	n-C$_6$ µL/L	McC$_5$ µL/L	n-C$_7$ µL/L	McC$_6$ µL/L	C$_1$/C$_2$+C$_3$	iC$_4$/nC$_4$	iC$_5$/nC$_5$
2535	440	0.00	0.01	0.05	0.16	0.00	0.15	0.50	150	1.33	0.83
2535	590	0.01	0.03	0.08	0.20	0.05	0.36	0.46	164	2.10	3.54
2535	1,190	0.00	0.02	0.00	0.00	0.00	0.00	0.00	292		
2535	2,390	0.75	1.15	0.29	0.46	0.37	0.09	0.30	2,376	4.90	5.94
2535	2,690	5.03	6.50	0.49	0.42	2.49	0.00	0.00	154	7.11	
2535	2,840	0.00	0.04	0.08	0.20	0.00	0.45	0.49	23,318	0.89	1.61
2537	440	0.00	0.02	0.09	0.32	0.04	0.41	0.49	775	1.37	2.17
2537	890	0.00	0.00	0.00	0.00	0.00	0.00	0.00	211	0.39	
2537	1,640	0.03	0.19	0.41	0.00	1.03	0.84	1.17	436	0.76	3.69
2537	2,090	0.00	0.01	0.05	0.12	0.00	0.15	0.28	783	0.84	2.06
2537	3,240	0.00	0.10	0.46	0.50	0.86	0.58	0.87	678	1.01	4.48
2538	140	0.00	0.00	0.00	0.00	0.00	0.00	0.00	12	0.00	
2538	290	0.02	0.08	0.21	0.33	0.77	0.82	1.10	14	0.94	2.36
2538	440	0.05	0.06	0.17	0.42	0.12	0.73	0.98	139	1.44	2.54
2538	590	0.00	0.00	0.09	0.22	0.00	0.00	0.00	341	0.30	1.50
2538	740	0.00	0.00	0.00	0.00	0.00	0.00	0.00	513	0.37	
2539	140	0.00	0.00	0.00	0.08	0.00	0.00	0.00	40		
2539	890	0.00	0.00	0.00	0.07	0.00	0.00	0.00	42	0.00	
2539	1,640	0.00	0.00	0.00	0.07	0.00	0.00	0.00	30,118	0.39	
2539	2,390	0.06	0.08	0.30	0.00	1.25	0.94	1.60	26,064	1.35	3.10
2539	2,990	0.00	0.00	0.00	0.04	0.00	0.00	0.00	30,561	0.00	
2541	130	0.00	0.00	0.06	0.11	0.21	0.22	0.25	72		
2541	740	0.00	0.00	0.00	0.03	0.00	0.00	0.00	35	0.00	0.00
2541	1,490	0.00	0.00	0.00	0.00	0.44	0.00	0.00	46,354	0.00	1.57
2541	2,240	0.00	0.03	0.12	0.23	0.44	0.49	0.52	41,208	0.54	2.32
2543	900	1.64	5.84	1.81	0.18	0.62	1.03	0.38	395	6.34	21.42
2545	200	0.00	0.00	0.00	0.10	0.00	0.00	0.00	1,686	0.33	0.95
2545	390	0.00	0.00	0.00	0.06	0.00	0.00	0.00	1,190	0.66	4.12
2545	500	0.00	0.00	0.02	0.05	0.00	0.00	0.00	908	0.56	6.33
2545	690	0.03	0.08	0.24	0.31	0.64	0.60	0.75	564	0.67	4.71
2545	890	0.00	0.02	0.06	0.14	0.00	0.00	0.00	1,379	0.44	3.55
2546	140	0.00	0.00	0.00	0.30	0.16	0.19	0.14	747	0.40	2.81
2546	740	0.02	0.08	0.19	0.26	0.47	0.53	0.73	542	1.10	4.63
2546	1,340	0.00	0.02	0.00	0.03	0.00	0.00	0.00	438	0.73	2.57
2546	1,790	0.04	0.13	0.48	0.50	0.77	0.70	0.87	655	0.98	3.31
2546	2,240	0.01	0.00	0.00	0.12	0.00	0.00	0.00	1,371	0.64	1.72
2546	2,990	0.04	0.05	0.00	0.04	0.00	0.03	0.00	669	0.81	3.27

Table 2. Composition of hydrocarbon gas and carbon dioxide of core samples. — Continued

[c, centimeter; µL/L, microliter per liter; M, microbial; X, mainly microbial methane with some thermogenic hydrocarbons; TX, mainly thermal hydrocarbons with some microbial methane]

Core	Depth (cm)	$2,2MC_4$ µL/L	$2MC_5$ µL/L	$3MC_5$ µL/L	n-C_6 µL/L	McC_5 µL/L	n-C_7 µL/L	McC_6 µL/L	C_1/C_2+C_3	iC_4/nC_4	iC_5/nC_5
2553	2,814	0.00	0.00	0.02	0.14	0.00	0.08	0.05	166	0.97	0.26
2554	140	0.02	0.01	0.17	0.44	0.10	0.44	0.72	1,680	0.48	1.11
2554	300	0.00	0.00	0.04	0.21	0.00	0.00	0.00	294	0.50	
2554	600	0.00	0.00	0.11	0.50	0.00	0.00	0.00	1,828	0.16	0.95
2554	2,065	0.07	0.22	0.57	0.70	0.75	0.95	0.98	527	0.33	1.94
2554	2,665	0.00	0.01	0.05	0.15	0.00	0.00	0.00	476	0.39	1.94
2555	600	0.00	0.00	0.05	0.32	0.00	0.00	0.00	1,434	0.20	1.19
2555	740	0.00	0.00	0.04	0.21	0.00	0.00	0.00	528	0.24	0.62
2555	2,240	0.00	0.00	0.05	0.15	0.00	0.00	0.00	5,339	0.23	1.19
2556	1,490	0.17	0.26	0.42	0.47	0.45	0.31	0.49	1,769	0.44	2.39
2556	2,090	0.44	1.72	2.74	4.33	0.72	5.36	7.88	1,123	0.19	2.01
2556	2,990	0.01	0.03	0.07	0.22	0.04	0.36	0.52	3,410	0.35	
2556	3,740	0.00	0.00	0.09	0.27	0.28	0.10	0.23	3,008	0.54	
2559	740	0.00	0.00	0.00	0.00	0.00	0.00	0.00	12	0.00	0.02
2559	1,450	0.05	0.07	0.18	0.29	0.12	0.50	0.61	16	1.10	1.88
2559	2,090	0.00	0.01	0.06	0.15	0.00	0.28	0.47	2,081	1.76	1.43
2559	2,840	0.01	0.06	0.20	0.36	0.31	0.26	0.30	24	0.38	2.85
2559	3,290	0.00	0.02	0.12	0.22	0.14	0.11	0.14	18	0.44	2.50
2560	140	0.00	0.02	0.12	0.24	0.21	0.16	0.24	89	1.08	2.42
2560	730	0.00	0.00	0.02	0.08	0.00	0.18	0.11	1,281	2.22	1.92
2560	1,490	0.00	0.00	0.00	0.11	0.00	0.00	0.00	9	0.68	0.40
2560	2,090	0.00	0.03	0.12	0.20	0.23	0.13	0.22	139	0.99	2.72
2561	590	0.00	0.00	0.00	0.08	0.00	0.00	0.00	116	0.81	0.44
2561	1,180	0.06	0.05	0.11	0.38	0.55	0.83	0.81	100	0.47	1.16
2561	1,790	0.00	0.01	0.03	0.12	0.01	0.18	0.29	9	0.52	5.67
2561	2,390	0.02	0.03	0.13	0.32	0.08	0.40	0.61	196	1.50	2.94
2561	2,840	0.04	0.19	0.71	0.59	0.62	0.78	0.93	13	0.29	2.00
2562	440	0.00	0.01	0.04	0.11	0.00	0.20	0.35	56	1.37	
2562	730	0.00	0.06	0.23	0.39	0.32	0.25	0.43	7	0.44	2.42
2562	890	0.00	0.05	0.11	0.28	0.05	0.50	0.82	165	1.32	2.51
2562	1,490	0.00	0.02	0.11	0.00	0.20	0.23	0.24	12	0.66	2.20
2562	2,090	0.00	0.01	0.03	0.00	0.02	0.16	0.30	26	1.57	5.50
2562	2,450	0.16	1.22	1.11	2.91	0.28	1.87	1.31	7	0.26	0.78
2563	90	0.77	1.25	1.93	2.19	1.62	3.79	2.75	17	0.57	1.90
2563	295	9.00	4.88	0.52	0.46	0.33	0.00	0.25	49	2.79	6.64
2563	380	35.11	71.64	5.46	2.77	1.92	0.00	1.20	25	10.34	21.16

Table 2. Composition of hydrocarbon gas and carbon dioxide of core samples. — Continued

[c, centimeter; µL/L, microliter per liter; M, microbial; X, mainly microbial methane with some thermogenic hydrocarbons; TX, mainly thermal hydrocarbons with some microbial methane]

Core	Depth (cm)	2,2MC$_4$ µL/L	2MC$_5$ µL/L	3MC$_5$ µL/L	n-C$_6$ µL/L	McC$_5$ µL/L	n-C$_7$ µL/L	McC$_6$ µL/L	C$_1$/C$_2$+C$_3$	iC$_4$/nC$_4$	iC$_5$/nC$_5$
2565	440	44.02	95.65	113.69	104.27	39.05	97.70	83.87	3	3.05	4.74
2565	890	58.43	143.10	285.10	159.20	133.63	181.45	151.53	8	0.21	4.25
2565	1,190	35.53	116.88	109.62	108.42	24.83	87.76	88.52	5	0.52	1.87
2565	1,640	27.65	119.26	106.27	122.31	25.16	112.58	67.31	7	0.36	1.64
2565	2,240	6.28	28.60	26.23	32.55	2.95	14.61	8.53	13	0.46	1.28
2566	440	0.01	0.02	0.06	0.19	0.02	0.31	0.38	10	1.84	1.28
2566	890	0.00	0.01	0.04	0.19	0.00	0.11	0.18	11	0.45	0.69
2566	1,340	0.00	0.01	0.05	0.16	0.02	0.29	0.48	20	1.51	1.43
2566	1,940	0.00	0.01	0.03	0.13	0.01	0.19	0.24	10	0.32	7.07
2566	2,390	0.00	0.01	0.05	0.24	0.02	0.20	0.49	18	0.50	3.88
2567	590	0.00	0.01	0.06	0.18	0.03	0.33	0.58	17	1.54	1.73
2567	1,340	0.43	2.70	2.28	5.13	0.35	2.33	2.06	3	0.28	0.93
2567	1,490	0.00	0.03	0.07	0.19	0.00	0.28	0.47	43	0.82	5.00
2567	1,790	0.11	0.90	0.76	2.15	0.23	1.63	1.02	6	0.21	0.78
2567	2,090	0.00	0.03	0.16	0.26	0.26	0.16	0.29	22	1.04	9.50
2569	995	0.17	0.89	0.02	8.03	8.01	0.37	0.00	184	201.08	5.77
2569	1,400	0.13	0.74	2.49	1.79	1.00	1.37	1.43	296	0.19	1.62
2569	1,640	0.00	0.00	0.00	0.18	0.00	0.00	0.00	597	0.77	1.31
2569	2,090	0.04	0.23	0.82	0.72	0.63	0.75	0.76	1,110	0.31	1.82
2569	2,690	2.39	10.46	9.95	10.81	2.32	10.86	7.32	22	0.30	1.90
2570	440	0.02	0.05	0.16	0.32	0.07	0.56	0.71	950	1.02	2.14
2570	1,040	0.00	0.10	0.07	0.12	0.00	0.41	0.45	1,644	0.61	0.70
2570	1,490	0.27	0.76	1.85	1.45	1.56	1.79	2.25	249	0.45	2.64
2570	1,790	0.00	0.00	0.00	0.11	0.00	0.33	0.00	695	0.86	0.72
2570	2,240	0.04	0.16	0.64	0.66	0.57	0.74	1.01	479	0.62	2.41
2573	260	2.90	1.94	0.37	0.84	0.89	0.00	0.45	261	1.87	3.99

Table 2. Composition of hydrocarbon gas and carbon dioxide of core samples. — Continued

[c, centimeter; µL/L, microliter per liter; M, microbial; X, mainly microbial methane with some thermogenic hydrocarbons; TX, mainly thermal hydrocarbons with some microbial methane]

Core	Depth (cm)	C_1 $\delta^{13}C$	CO_2 $\delta^{13}C$	C_2 $\delta^{13}C$	C_3 $\delta^{13}C$	i-C_4 $\delta^{13}C$	n-C_4 $\delta^{13}C$	C_5 $\delta^{13}C$	Source
2535	440								M
2535	590	-94.62	-26.52						M
2535	1,190								M
2535	2,390								M
2535	2,690	-93.11	-21.87						X
2535	2,840								M
2537	440								M
2537	890								M
2537	1,640	-66.00	-18.00						M
2537	2,090								M
2537	3,240	-74.30	-20.11						M
2538	140								M
2538	290								M
2538	440	-74.50	-45.40						M
2538	590	-71.00	-34.40						M
2538	740	-81.70	-19.70						M
2539	140								M
2539	890								M
2539	1,640	-96.60	-33.10						M
2539	2,390								M
2539	2,990								M
2541	130								M
2541	740								M
2541	1,490	-97.10	-26.70						M
2541	2,240								M
2543	900	-61.20	-3.00						X
2545	200	-98.30	-43.40						X
2545	390								X
2545	500								X
2545	690	-62.60	-15.20						X
2545	890								X
2546	140	-81.90	-21.20						M
2546	740								M
2546	1,340	-75.60	-27.90						X
2546	1,790								X
2546	2,240								X
2546	2,990	-70.80	-11.70						X

Table 2. Composition of hydrocarbon gas and carbon dioxide of core samples. — Continued

[c, centimeter; µL/L, microliter per liter; M, microbial; X, mainly microbial methane with some thermogenic hydrocarbons; TX, mainly thermal hydrocarbons with some microbial methane]

Core	Depth (cm)	C_1 $\delta^{13}C$	CO_2 $\delta^{13}C$	C_2 $\delta^{13}C$	C_3 $\delta^{13}C$	i-C_4 $\delta^{13}C$	n-C_4 $\delta^{13}C$	C_5 $\delta^{13}C$	Source
2553	2,814	-45.67	-23.81						M
2554	140	-83.24	-29.22						M
2554	300	-75.00	-10.40						X
2554	600	-91.10	-43.40						X
2554	2,065								X
2554	2,665								X
2555	600								X
2555	740								M
2555	2,240								M
2556	1,490	-85.89	-24.38						X
2556	2,090	-72.82	-20.19						X
2556	2,990	-84.08	-20.78						M
2556	3,740	-81.01	-14.22						M
2559	740								M
2559	1,450								M
2559	2,090	-64.09	-15.94						M
2559	2,840								M
2559	3,290								M
2560	140								M
2560	730	-93.59	-20.88						M
2560	1,490								M
2560	2,090	-72.00	-18.57						M
2561	590								M
2561	1,180								M
2561	1,790								M
2561	2,390	-62.56	-22.51						M
2561	2,840								M
2562	440								M
2562	730								M
2562	890	-72.12	-20.61						M
2562	1,490								M
2562	2,090								M
2562	2,450								M
2563	90								TX
2563	295	-53.11	-12.07	-28.15					TX
2563	380	-52.22	-2.23	-28.18	-18.53				TX

Table 2. Composition of hydrocarbon gas and carbon dioxide of core samples. — Continued

[c, centimeter; µL/L, microliter per liter; M, microbial; X, mainly microbial methane with some thermogenic hydrocarbons; TX, mainly thermal hydrocarbons with some microbial methane]

Core	Depth (cm)	C_1 $\delta^{13}C$	CO_2 $\delta^{13}C$	C_2 $\delta^{13}C$	C_3 $\delta^{13}C$	i-C_4 $\delta^{13}C$	n-C_4 $\delta^{13}C$	C_5 $\delta^{13}C$	Source
2565	440								TX
2565	890								TX
2565	1,190	-60.10	-11.10	-28.83	-26.40	-28.44	-25.94	-26.01	TX
2565	1,640	-58.87	-3.93	-29.48	-27.63	-28.55	-26.45	-26.51	TX
2565	2,240	-59.88	-11.15	-28.96	-26.18		-25.49		TX
2566	440								M
2566	890								M
2566	1,340								M
2566	1,940								M
2566	2,390								M
2567	590								M
2567	1,340								M
2567	1,490								M
2567	1,790								M
2567	2,090								M
2569	995	-59.52	-2.71						X
2569	1,400	-70.52	-21.33						X
2569	1,640	-67.02	-11.40						X
2569	2,090	-67.81	-11.55						X
2569	2,690	-62.02	-42.48						X
2570	440	-72.35	-28.58						X
2570	1,040	-68.74	-13.98						X
2570	1,490	-67.14	-11.76						X
2570	1,790	-66.55	-10.85						M
2570	2,240	-66.38	-14.03						X
2573	260	-62.11	-18.66	-30.08					X